Challenge Journal of
STRUCTURAL MECHANICS

Vol.8 No.2 (2022)

Mindlin's theory buckling columns compressive strength dynamic analysis dynamic response earthquake finite element analysis finite element method mechanical properties metaheuristic algorithms modal analysis natural frequency optimization pushover analysis reinforced concrete seismic analysis seismic design seismic isolation steel silo teaching-learning based optimization [illegible]plate

TULPAR ACADEMIC PUBLISHING

ISSN 2149-8024

Challenge Journal of Structural Mechanics

E-mail: *cjsmec@challengejournal.com*

Web page: *cjsmec.challengejournal.com*

TULPAR Academic Publishing
www.tulparpublishing.com

Challenge Journal of Structural Mechanics

CONTENTS

Research Articles

TULPAR ACADEMIC PUBLISHING

Challenge Journal of Structural Mechanics

Research Article

Effect of carbon fibers on the mechanical properties of steam-cured concrete

Mehmet Canbaz [a,*], Mouad Bensaoud [b], Hakan Erol [a], H. Selim Şengel [a]

[a] *Department of Civil Engineering, Eskişehir Osmangazi University, 26480 Eskişehir, Turkey*
[b] *Department of Civil Engineering, University of Tripoli, R6XF+46G Tripoli, Libya*

ABSTRACT

While the use of the steam-curing method in the precast concrete can result in an early high compressive strength and thus can increase the production rate of structural elements, it should be noted that the steam-curing method has some negative effects on the mechanical properties of concrete due to the fact that the high-temperature steam causes micro-cracks. On the other hand, the inclusion of carbon fibers enhanced the overall mechanical properties in terms of high tensile strength and modulus of elasticity. This paper aimed to investigate the effect of adding carbon fibers to steam-cured concrete. Twenty-seven cube specimens of 15 cm dimensions were used to investigate the unit weights, the ultrasonic pulse velocity, the compressive strength, and the split tensile strength of the concrete. Three different mixes were made by adding carbon fibers (0%, 0.12% and 0.24%) by weight to the concrete. Three of each were kept in a standard curing environment for 3, 7 and 28 days. Three specimens of each mix were steam-cured for 4 hours, and three specimens were steam-cured for 8 hours. The result showed a significant increase in the rate of gaining compressive strength under steam-curing with an enhancement in the tensile strength due to the presence of fibers, all without compromising the integrity of the concrete and without increasing the amount of voids.

ARTICLE INFO

Article history:
Received 14 January 2022
Revised 21 February 2022
Accepted 1 March 2022

Keywords:
Fiber carbon
Steam-curing
Precast
Fiber reinforced concrete

1. Introduction

As a result of the rapid development around the world, there is always a need to build structures at a lower cost and in a shorter time without compromising the quality. Therefore, researchers focus on developing the production process of structural elements rather than relying on improving project execution techniques. Using precast concrete is one of the best ways to achieve this in reinforced concrete structures (Ba et al. 2011). One of the main advantages of precast concrete is to increase the production rate in many ways. One of the most cost-effective ways is by accelerating the concrete curing process (Shi et al. 2020; Hanif et al. 2017).

Various methods are used for accelerating the concrete hardening process, to gain higher early-age performance. Steam-curing is one of the most widely used accelerated curing methods, which proved numerous advantages in terms of the material characteristics such as less permeability, intent microstructures, high mechanical properties, and more hydrated products at early stages (Ba et al. 2011). However, the steam curing method demonstrated disadvantages in terms of long-term compressive strength, micromechanical properties. Based on Liu et al. (2020), a dense region around the cement particles formed as a result of the rapid hydration caused by the steam curing heating result in an expansion of the gas-liquid phase inside the concrete which produces micro-cracks.

One of the methods used to improve the mechanical properties of concrete is to add fibers to the concrete mix (Yang et al. 2017; Guo et al. 2021). Fiber admixture con-

* *Corresponding author*. Tel.: +90-222-239-3750 ; Fax: +90-222-239-3613 ; E-mail address: mcanbaz@ogu.edu.tr (M. Canbaz)
ISSN: 2149-8024 / DOI: https://doi.org/10.20528/cjsmec.2022.02.001

tributes to increasing the concrete's resistance to compressive and tensile loads, as well as its resistance to cracks expansion. The behavior of fiber reinforced concrete varies according to the type, length, and density of the fibers used (Zhang et al. 2019). Considering its corrosion and high-temperature resistance, as well as high tensile strength and modulus of elasticity, carbon fiber is recommended over other types of fibers.

The effect of fibers on the behavior of concrete has been tested by many researchers. According to Mastali et al. (2017), the mechanical properties of fiber reinforced concrete, as well as the impact resistance, can be improved by increasing the length of carbon fiber and the volume fraction. (Rangelov et al. 2016) investigated the differential impact of carbon fiber sizes and combine them with cement mortar mixtures. The result showed an increase by (4–11%) of the 28-day compressive strength and 7-day tensile strength increased by (11–46%). Xiong et al. (2019) demonstrated that when carbon fiber dosage increases a clear improvement in Vickers hardness, fracture toughness, and the ultimate capacity when they studied the mechanical behavior of carbon fiber reinforced concrete. Yakhlaf et al. (2013) investigated carbon fibers effect on the physical properties of self-consolidating concrete. The study concluded that (filling ability and passing ability) inversely correlated with the amount of carbon fibers. However, the amount of carbon fibers had no negative impact on the segregation resistance of concrete.

On the other hand, other studies focused on the mechanical properties of carbon fiber reinforced concrete that has been exposed to high temperatures. The effect of post high temperature on the elastic modulus, compressive strength, and toughness of fiber reinforced concrete have been researched by Dügenci et al. (2015). The study found that 1.0% fiber additive had a minimum loss of compressive strength of fiber reinforced concrete that exposed to a high temperature. Varona et al. (2018) and Wang et al. (2021) suggested a formula to the progression of mechanical behavior post exposure to high temperatures, as a result of their investigation of the mechanical behavior of fiber reinforced concrete,

Most of the above-mentioned studies focus on investigating the mechanical properties of fiber reinforced concrete under standard curing conditions or after exposure to high temperatures, while carbon fiber reinforced concrete was not investigated under steam curing conditions. This paper aims to investigate the effect of steam curing on the compressive strength, the Ultrasonic pulse velocity, unit weights, and the split tensile strength of concrete for cubic specimen of concrete reinforced with different ratios of carbon fibers under different steam curing periods and comparing it with specimens tested 28 days later under standard curing conditions.

2. Experimental Study

2.1. Materials

Three types of crushed aggregates were used in casting concrete cube specimens. The particle size analysis of the aggregate mixture used can be seen in Fig. 1. The density of the fine aggregate of sizes (0-4 mm), (4-11.2 mm) and (11.2-22.4 mm) were 2.69, 2.70 and 2.71 g/cm^3, respectively.

Table 1 shows the properties of the new generation of superplasticizers that were used as an admixture for the concrete.

Carbon fibers added to the concrete mix are shown in Fig 2. The properties of fibers are given in Table 2. The fibers have been used up to 0.24% by weight of the concrete.

The type of cement used is CEM I.42.5 R Portland cement, the chemical and physical properties of the cement used are given in Table 4. Tap water was used for mixing the specimen, the physical and chemical properties of the water used can be shown in Table 3.

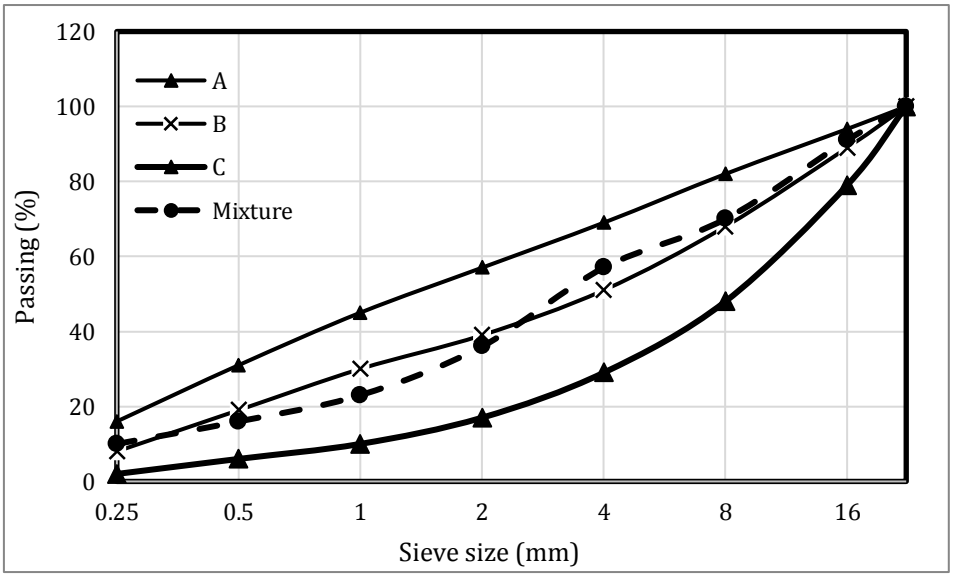

Fig. 1. Granulometry of aggregate mixture according to EN 12620.

Table 1. Properties of admixture.

Chemical Structure	Appearance	Cl, %	pH	Density, g/cm³	Alkali, %
Polycarboxylic ether	Brown	≤ 0.10	5-7	1.069-1.109	≤ 3.00

Table 2. Properties of carbon fiber.

Tensile Str., MPa	Tensile Mod., GPa	Strain, %	Density, g/cm³	Yield, g/1000m
240	4200	1.8	1.78	800

Fig. 2. Carbon fiber.

Table 3. Properties of mixing water.

Chemical Property, mg/l						Physical property	
Al	0.04	Cu	0.016	Ni	5.07	Conductivity, µS/cm	628
NO_3	11.1	Fe	0.007	K	6.8	Hardness, Fd^0	30.11
NH_4	0.06	Mn	0.015	As	1.19	pH	7.35

Table 4. Properties of cement.

Chemical properties				Physical properties	
SiO_2	19.20	K_2O	0.63	Density, g/cm³	3.09
Al_2O_3	4.56	Na_2O	0.31	Specific surface, cm²/g	3190
Fe_2O_3	3.09	SO_3	3.21	Setting Time(initial), min	163
CaO	62.90	CI-	0.01	Setting Time(final), min	228
MgO	1.88	LOI	3.80	Soundness, mm	1

2.2. Method and tests

The concrete was mixed according to the ratios given in Table 5. Three different mixes were made by adding carbon fibers (0%, 0.12% and 0.24%) by weight to the concrete mixture as can be seen in Fig 3. Cube specimens of 15 cm dimensions were cast. Nine specimens of each mix were cast, three of each were kept in a standard curing environment for 3, 7 and 28 days. Three specimens of each mix were steam cured for 4 hours, and three specimens were steam cured for 8 hours.

Table 5. Mix ratio of 1 m³ of concrete mixture.

Cement, kg	Water, l	Superplasticizer, l	Aggregate, kg		
			0-4 mm	4-11.2 mm	11.2-22.4 mm
435	125	3.5	967	333	555

At the end of the curing process, unit weight, ultrasonic pulse, split tensile strength and compressive tests were carried out on the specimens as shown in Fig 4. Examination of the changes in the unit weight, ultrasonic pulse velocity, splitting tensile strength and compressive strength for each fiber ratio, curing condition and curing duration was carried out and the results will be discussed in further sections.

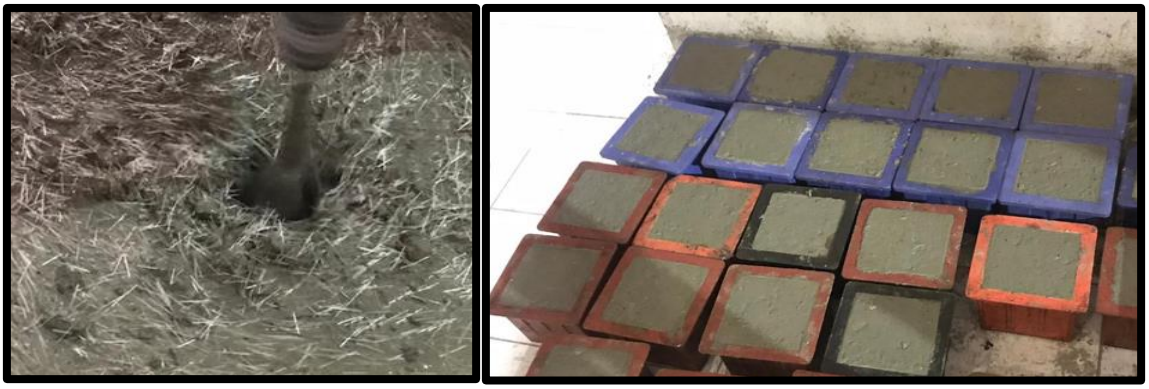

Fig. 3. Adding carbon fiber to the fresh concrete (left), and cube specimens (right).

Fig. 4. Ultrasonic pulse velocity and mechanical tests.

Fig. 5. Steam curing.

3. Discussion

Average unit weight test results are shown in Fig 6. Specimen unit weights varied from 2407 to 2480 kg/m^3. As it can be seen from the figure, the increase in the fibers caused the unit weight values to increase. In 0.12% fiber concrete mix, the unit weights of the specimens increased by 1.4% compared to the mix without fibers, while in 0.24% fiber concrete mix, the increase in unit weights reached 2.1%. Moreover, since the fiber addition affects the workability of the fresh mix, the voids formed during the setting caused the unit weights to increase at different rates for each fibre content. As the curing time increased, the unit weights for fibrous specimens increased up to 2.2%, which is a significant increase compared to the non-fibrous specimens. The increase in unit weight was caused by the formation of cement reaction structures that filled the voids.

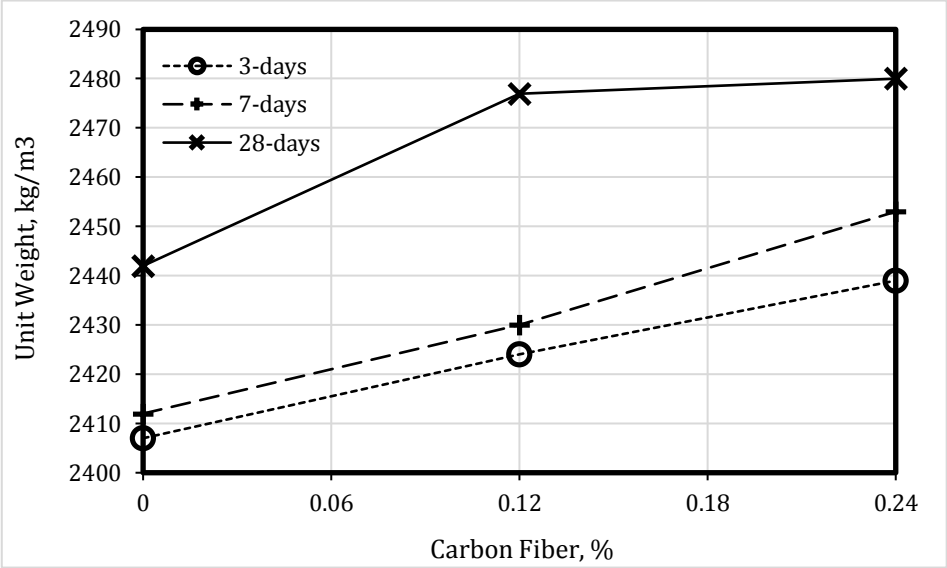

Fig. 6. The effect of fiber ratio on unit weights of concrete specimens.

Changes in ultrasonic pulse velocity for carbon fiber content mix are shown in Fig 7. It can be noted that the ultrasonic pulse velocities were increased with increasing carbon fiber content. While this increase was 0.9% in the case of 0.12% carbon fiber mix, the increase rate reached 5.7% when the carbon fiber ratio was 0.24%. This increase can be due to fibers acting as bridges, allowing ultrasound vibrations to be transmitted through the fibers instead of being transmitted through the pores. As the curing time increased, the ultrasonic pulse velocities increased up to 4.7%, this might be caused by filling of the voids by the hydration reaction products formed over a longer hydration time. The highest ultrasonic pulse velocity value was observed in specimens containing 0.24% fiber for 28 days, the increase in ultrasonic pulse velocities with the increase in fiber content was more pronounced in specimens tested after 28 days.

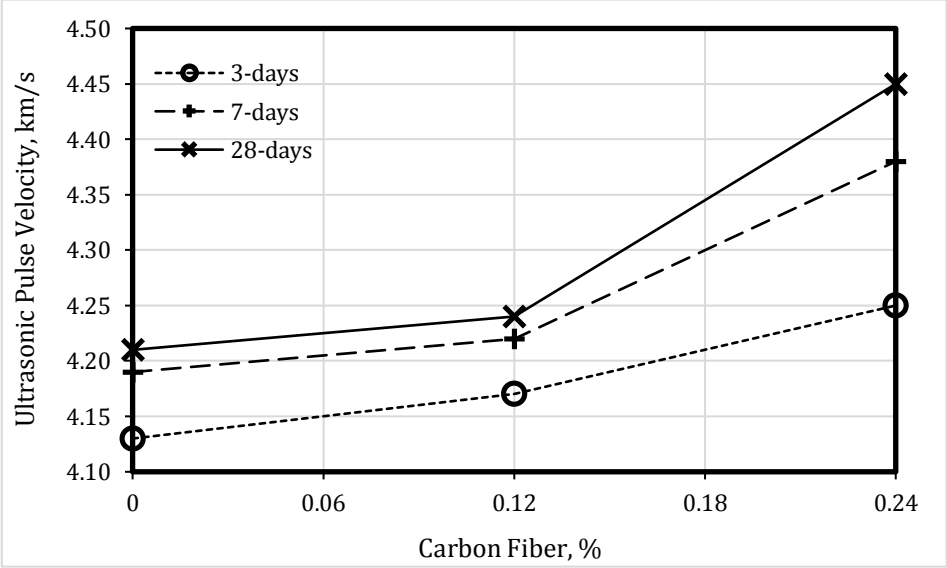

Fig. 7. The ultrasonic pulse velocity rate of concrete under various carbon fiber ratios.

The resulting compressive strength values for each curing time and fiber content can be seen in Fig 8. Compressive strength results were shown to increase with increasing fiber content, this was caused due to the crack growth and branching of micro-cracks formed as the loads were increased in the fiberous mix specimens. While this increase was 7.6% in the case of using 0.12% fiber, the strength reached 14.2% in the 0.24% fiber mix. Examination of the changes of the compressive strength with the curing time showed that the specimens reached 64.1% of the 28-day compressive strength on the 3rd day, and 81.7% on the 7th day. It can also be observed that in the case of 0.24% fiber content mix, the effect of increasing the fiber content is more notable at early ages.

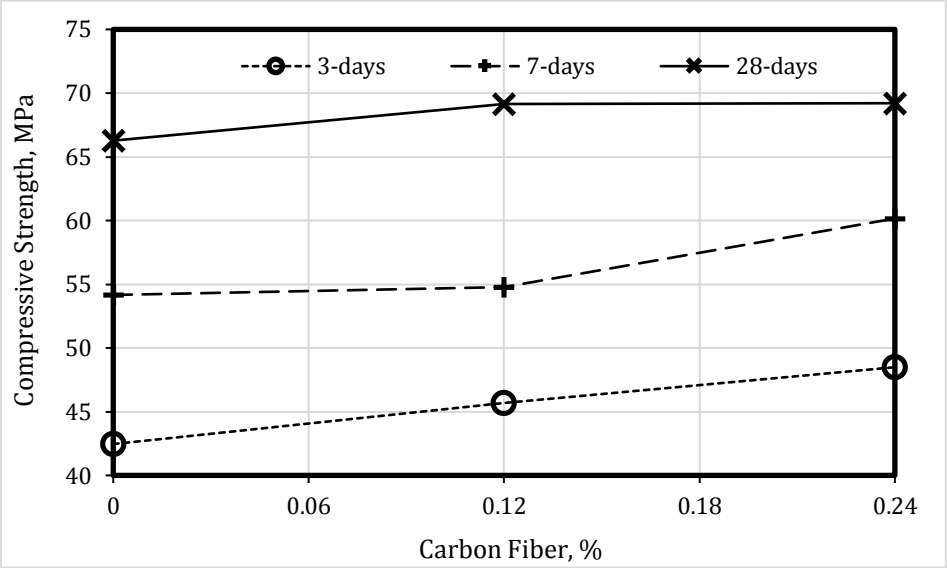

Fig. 8. The compressive strength of concrete under various carbon fiber ratios.

Variation in split tensile strengths for the mixes are shown in Fig. 9. It can be seen that the increase in splitting tensile strength of the specimens increased by 12.1% when the fiber ratio was 0.12%, while it reached a 23.1% increase when the fiber ratio was 0.24%. Due to the brittleness of concrete, there is a sudden loss of strength, particularly after the development of the first crack under the tensile effect. Although the fibers could not prevent the formation of the first crack, they prevent the crack growth and propagation until fibers lose their bond with the binder. This explains the increase in splitting tensile strengths. Therefore, the use of fibers is advantageous as it reduces the brittleness of the concrete mixture under tensile stresses. Cement hydration reactions over time caused an increase in the calcium silicate hydrate gels, this not provided compressive strength gains but also enhanced the tensile strength, which explains the increase in the tensile strength over longer curing times. The tensile strength of the fibrous mixes significantly had a significant enhancement in early splitting strength, a similar effect was noted in the compressive strength behavior discussed earlier. However, unlike compressive strength, the increase in fiber ratio caused a significant increase in splitting tensile strength in 28 days.

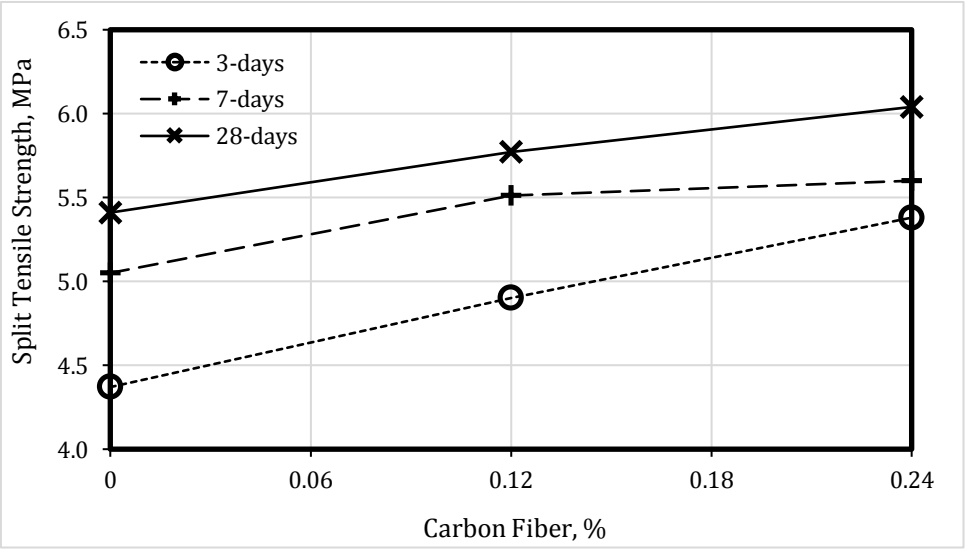

Fig. 9. The split tensile strength of concrete under various carbon fiber ratios.

Variation of unit weight values under the effect of steam curing for each mix are shown in Fig. 10. While the unit weights of the steam cured specimens reached 98% of the reference specimen, a negligible increase of 0.4% was observed in the unit weights of the specimens with the increase in the steam curing application time, therefore there was no negative effect of steam curing on the unit weights of the specimens. It also should be noted that with the increase in the fiber content with steam curing, the unit weights of the specimens increased by 1.3%.

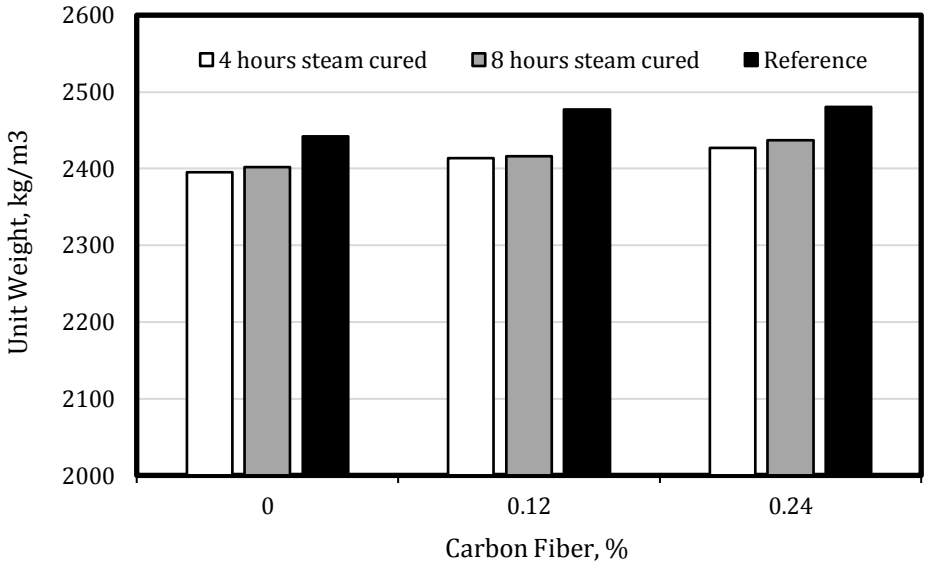

Fig. 10. Comparing the unit weight of steam-cured concrete under various curing durations and carbon fiber ratios to the reference specimens.

Variation of ultrasonic pulse velocity of specimens with steam curing time and fiber ratio is shown in Fig 11. The ultrasonic pulse velocity of the 4 hours steam cured specimens was 95.7% of the ultrasonic pulses of the reference specimen, while this rate reached 97.9% when the steam curing time was 8 hours. With the increase in fiber content, there was a decrease in the variation between the ultrasonic pulse velocity for different steam curing application times, notably for fiber content of 0.24%, this rate decreased to 0.2%. However, a decrease in rates up to 6.4% was observed for the specimen of steam cured specimens with fiber content of 0.24% compared to the reference specimen. This effect might be due to the increase in the hydration reaction rate in the concrete with the application of steam curing, causing the filling of the internal structure and the formation of cement products in a short time, which in turn caused a significant rate of ultrasonic pulse velocities compared to the reference.

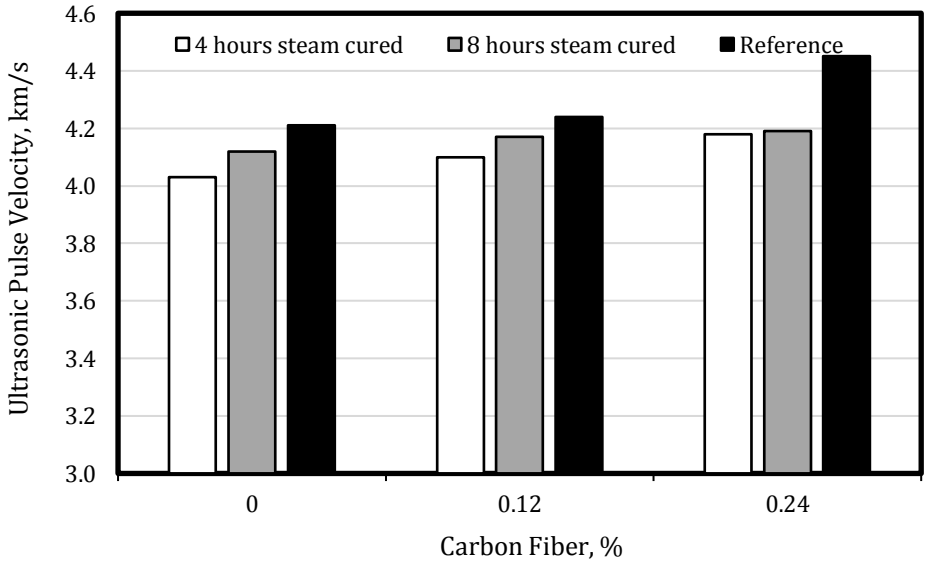

Fig. 11. The ultrasonic pulse velocity rate of steam-cured concrete under various carbon fiber ratios.

In Fig. 12, the change in compressive strength of specimens with fiber ratio and steam curing time are shown. In the case of the compressive strengths of non-fibrous specimens, and when taking the compressive strength of the 28-day normal concrete as a reference, around 45.7% of this strength was reached when the 4 hours-steam curing was applied, and 56.7% of the compressive was reached when steam curing for 8 hours. In precast concrete applications, it is important to reach about half of the 28-day strength in a short time (e.g., 4 hours). The strengths obtained for steam cured specimens are accelerated by the effect of curing tempera-

ture due to the formation of calcium silicate hydrate gels with a more robust structure. In addition, the water loss that would have resulted due to this temperature is prevented as a result of the saturation of steam. In the case of different fiber content specimens, the 5% compressive strength increase in the reference specimens was reduced to 3% in steam cured specimens. When the steam curing time increased from 4 hours to 8 hours, the compressive strengths increased by 25% even when fibers are added. Therefore, increasing the steam curing time does not increase the strength at the same rate.

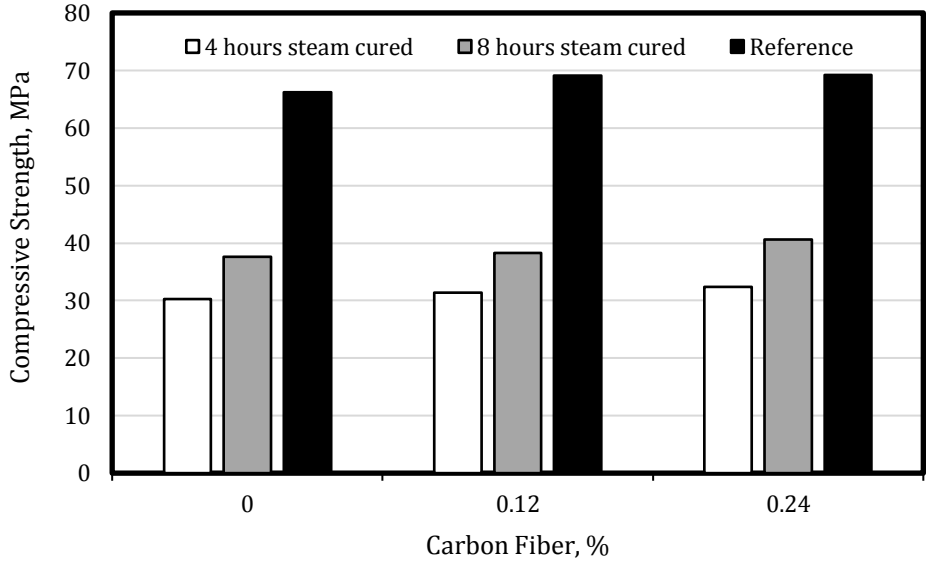

Fig. 12. The compressive strength of steam-cured concrete under various curing duration and carbon fiber ratios.

The effect of steam curing and carbon fiber ratio on the splitting tensile strength is illustrated in Fig. 13. An increase of 27% was observed in the split tensile strength of the fibrous specimens kept in steam curing for 4 hours, while the increase rate reached 17% in the specimens kept in steam curing for 8 hours. With the addition of fiber, crack control in the hardened cement paste was achieved. Although it is important to gain strength quickly with steam curing, particularly after the concrete has hardened, the split tensile strengths of the fibrous specimens with 4 hours and 8 hours steam curing gave close results. It is evident that the fibers have a very significant effect on the tensile effect, it can be observed that the split tensile strength of the non-fibrous specimens, which were steam cured for 4 hours, reached 47.5% of the split tensile strength of the reference concretes, while this ratio was 64.8% in the 8-hour steam curing.

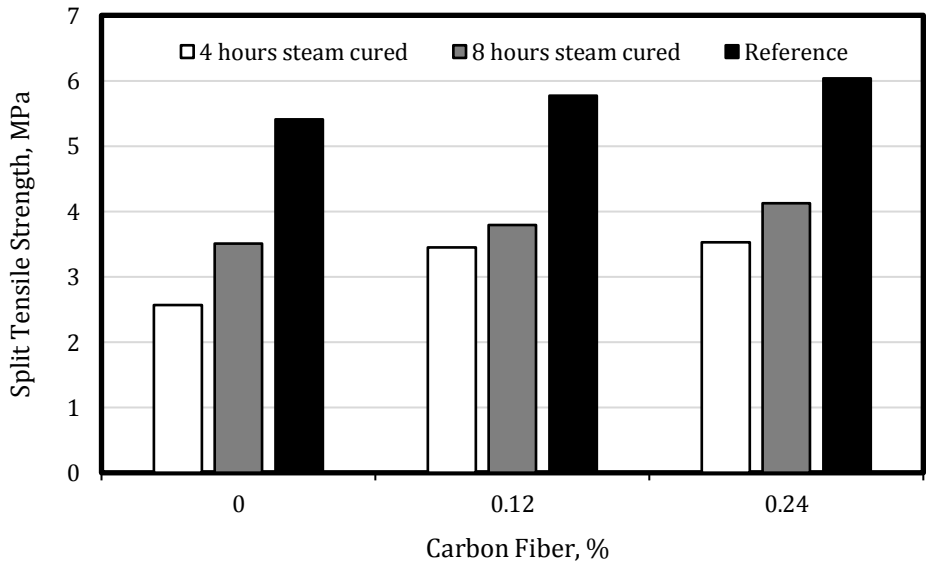

Fig. 13. The split tensile strength of steam-cured concrete under various curing duration and carbon fiber ratios.

4. Conclusions

The following results have been achieved with the experimental study conducted:

- The addition of carbon fiber increased unit weights, Ultrasonic pulse velocity, compressive strength, and split tensile strength of the concrete. Interestingly, the largest increase has occurred in the split tensile strength. The evidence from this study suggests to use 0.24% carbon fiber for tensile strength, while 0.12% fiber is sufficient for compressive strength. An implication of this is the possibility that carbon fiber can be used in places where strength is important at early ages, since fibers positively affect the mechanical properties of concrete at an early age.
- As the steam curing application time increased, very low increases were observed in the unit weights of the specimens, around 0.2%, and very low increases in the Ultrasonic pulse velocity around 2.2%. This finding suggests that steam curing does not impair the integrity of the concrete and does not increase the amount of voids. Steam curing is especially applied to improve the early age mechanical properties of concrete. This study has shown that as the steam curing time increased, the compressive strengths increased by 25% and the splitting tensile strengths increased by 36.5%. This study has also found that compressive strengths of 30 MPa have been reached with 4 hours of steam curing. According to the results of compressive strength under normal conditions, additional steam curing is not recommended unless very high compressive strength is required, since 8-hour steam curing does not increase much compared to 4-hour application.
- The unit weight of the specimens increased by 1.5%, the ultrasonic pulse velocity by 3.7%, the compressive strength by 8.2%, and the splitting tensile strength by 37%, with the increase in the carbon fiber ratio used in the steam cured specimens. While the effect of steam curing on the rate of gaining compressive strength is very high, it has been observed that it has a positive effect of the fibers on the tensile strength of the specimens. For the fact that stem curing imposes the precast elements under aggressive conditions, the use of carbon fiber is recommended to control cracks caused by internal tensile stresses that may arise from these effects.

The results of this study indicate that the addition of carbon fiber to improve the concrete mechanical properties did not adversely affect the strength gain rate under the effect of steam curing. While steam curing is highly preferred in the precast sector in practice, it has been observed that fibers are not used in the production of concrete or reinforced concrete elements. The results of this research support the idea of increasing the use of fibers in this sector, especially in order to increase the mechanical properties and crack control performance. A further study could assess the long-term effects of steam curing performance of fiber use and the control of cracks that may occur in an aggressive environment, especially in precast concrete, with fiber.

Acknowledgements

None declared.

Funding

The authors received no financial support for the research, authorship, and/or publication of this manuscript.

Conflict of Interest

The authors declared no potential conflicts of interest with respect to the research, authorship, and/or publication of this manuscript.

References

Ba M, Qian C, Guo X, Han X (2011). Effects of steam curing on strength and porous structure of concrete with low water/binder ratio. *Construction and Building Materials*, 25, 123-128.

Ba MF, Qian CX, Guo XJ, Han XY (2011). Effects of steam curing on strength and porous structure of concrete with low water/binder ratio. *Construction and Building Materials*, 25, 123–128.

Düğenci O, Haktanir T, Altun F (2015). Experimental research for the effect of high temperature on the mechanical properties of steel fiber-reinforced concrete. *Construction and Building Materials*, 75, 82–8.

Guo Z, Zhuang G, Li Z, Chen Y (2021). Mechanical properties of carbon fiber reinforced concrete (CFRC) after exposure to high temperatures. *Composite Structures*, 256, 0263-8223.

Hanif A, Kim Y, Lee K, Park C, Sim J (2017). Influence of cement and aggregate type on steam-cured concrete – an experimental study. *Magazine of Concrete Research*, 69(13), 694-702.

Liu B, Jiang J, Shen S, Zhou F, Shi J, He Z (2020). Effects of curing methods of concrete after steam curing on mechanical strength and permeability. *Construction and Building Materials*, 256, 0950-0618.

Mastali M, Dalvand A, Sattarifard A (2017). The impact resistance and mechanical properties of the reinforced self-compacting concrete incorporating recycled CFRP fiber with different lengths and dosages. *Composites Part B: Engineering*, 112, 74–92.

Rangelov M, Nassiri S, Haselbach L, Englund K (2016). Using carbon fiber composites for reinforcing pervious concrete. *Construction and Building Materials*, 126, 875–885.

Shi J, Liu B, Shen S, Tan J, Dai J, Ji R (2020). Effect of curing regime on long-term mechanical strength and transport properties of steam-cured concrete. *Construction and Building Materials*, 255, 119407, 1-10.

Varona FB, Baeza FJ, Bru D, Ivorra S (2018). Influence of high temperature on the mechanical properties of hybrid fiber reinforced normal and high strength concrete. *Construction and Building Materials*, 159, 73–82.

Wang B, Li C, Cao W (2021). Effect of polyacrylonitrile precursor orientation on the structures and properties of thermally stabilized carbon fiber. *Materials*, 14(12), 3237.

Xiong B, Wang Z, Wang C, Xiong Y, Cai C (2019). Effects of short carbon fiber content on microstructure and mechanical property of short carbon fiber reinforced Nb/Nb5Si3 composites. *Intermetallics*, 106, 59–64.

Yakhlaf M, Safiuddin M, Soudki KA (2013). Properties of freshly mixed carbon fiber reinforced self-consolidating concrete. *Construction and Building Materials*, 46, 224–31.

Yang JM, Yoo DY, Kim YC, Yoon YS (2017). Mechanical properties of steam cured high-strength steel fiber-reinforced concrete with high-volume blast furnace slag. *International Journal of Concrete Structures and Materials,* 11, 391–401.

Zhang X, Ge L, Zhang Y, Wang J (2019). Mechanical properties of carbon-fiber RPC and design method of carbon-fiber content under different curing systems. *Materials*, 12(22), 3759.

Challenge Journal of Structural Mechanics

Research Article

Performance-based assessment of long masonry structures

Ferit Cakir [a,*]

[a] *Department of Civil Engineering, Gebze Technical University, Gebze, 41400 Kocaeli, Turkey*

ABSTRACT

Performance-based assessment (PBA) has become an increasingly important concept for assessing the structural performance of existing structures today. This procedure aims primarily to determine structural damage subject to predetermined load effects and evaluate the state of the building based on the damage obtained. However, because of their complicated engineering characteristics and structural performance, it is very difficult to evaluate the performance of long masonry structures, such as aqueducts, castle ramparts and city walls. The PBA of long masonry structures is extremely challenging because there is no valid approach to assessing their performance. In this study, a practical evaluation method is developed to assess the structural performance of long structures and the seismic performance of Valens Aqueduct, which was constructed by the Roman Empire in Istanbul, is examined using this method.

ARTICLE INFO

Article history:
Received 23 January 2022
Revised 6 March 2022
Accepted 24 March 2022

Keywords:
Performance-based assessment
Seismic performance
Long masonry structures
Valentine aqueduct

1. Introduction

Masonry structures have been vulnerable to earthquakes by the nature of the brittle materials from which they were built. Therefore, most of the masonry structures built in seismic zones are damaged or collapsed as a result of earthquake effects. To improve the seismic performance of these structures, it is crucial to determine their performance-based seismic performance. For assessing the structural performance of structures, performance-based assessment (PBA) is considered a very important concept. The main objective of this approach is to determine structural damage when predetermined load effects are applied and to evaluate the condition of the building based on the damage obtained. Various standards and codes describe the PBA procedures for different types of structures, such as reinforced or unreinforced masonry structures (ASCE 41-17; FEMA 445-06; FEMA P-58; PERPETUATE-2010). Through linear or nonlinear evaluations, they can be used for assessing existing structures. When conducting seismic performance or damage assessment, several questions must be addressed: a) how to obtain structural drawings, specifically the structural details; b) how to determine the mechanical properties of the construction materials; and c) how to model and evaluate the structures.

How to model and evaluate the structures is the most controversial issue for engineering committees. Many researchers have discussed this topic and masonry structures are modelled and evaluated using several different methods. When the studies in the literature are examined, it is seen that many different building types are evaluated. Cakir (2021) developed a new simplified model to determine the structural performance of masonry structures. Gencer et al. (2020) investigated in-plane and out-of-plane wall behavior due to lateral loading, depending on wall profiles and opening types in Hellenistic towers. Preciado et al. (2015) performed damage analysis of a historic church in Mexico using the nonlinear finite element method. Korkmaz et al. (2015) focused on multi-story masonry structures and evaluated the structural performance of the historical Khatip School in Erzurum, Turkey. Cakir et al. (2015) performed performance evaluations on historical buildings damaged during the 2011 Van earthquake and performed performance analyses on two different historical buildings. Lagomarsino and Cattari (2015) conducted a seismic performance analysis of a historical masonry building using the performance evaluation method developed within the scope of the PERPETUATE project. Brandonisio et al. (2013) evaluated the performance of a masonry church during the 2009 L'Aquila earthquake.

* *Corresponding author*. Tel.: +90-262-605-1000 ; Fax: +90-262-653-8490 ; E-mail address: cakirf@gtu.edu.tr (F. Cakir)
ISSN: 2149-8024 / DOI: https://doi.org/10.20528/cjsmec.2022.02.002

Dogangun and Sezen (2012), considering the 1999 Kocaeli and Düzce earthquakes, examined the seismic performances of five different historical buildings and investigated the seismic weaknesses of the structures. Within the scope of a project called PERPETUATE, a performance-based approach has been proposed by Lagomarsino et al. (2010) for the protection of cultural heritage from earthquakes.

In particular, it is seen that the studies focused on the structures at the single structure scale, but the evaluation studies for the long structures are quite limited. Structures that have a relatively low height and a long length can be considered long structures. The stiffness of these structures is high along with in-plane directions but low along out-of-plane directions. The length of these structures can range from a hundred meters to many kilometers. Aqueducts, castle ramparts, and city walls are the best examples of these kinds of structures (Fig. 1). The evaluation of structural performances of long masonry structures is a very complex issue due to the lack of a valid method for assessing their performance. As part of this study, an evaluation method for the structural performance of long structures was developed, and the seismic performance of the Valens Aqueduct, which was constructed by the Roman Empire in Istanbul, was assessed by using this method.

Fig. 1. Some historical long structures (a) Xi'an City Wall, China; (b) Aurelian Walls, İtaly; (c) Aqueduct of Segovia, Spain; (d) Ávila City Wall, Spain; (e) Osaka Castle Rampart, Japan; (f) Diyarbakır City Wall, Turkey (images from Google Images).

2. Performance-Based Assessment of Long Masonry Structures

In determining the earthquake performance of masonry buildings, a simplified approach based on performance and calculation steps is given in Fig. 2. The PBA of a long structure starts with the seismic hazard assessment of the region and continues with setting the target performance levels and corresponding acceptance criteria, isolating a small segment of the structure, carrying out non-linear analyses on the isolated structure and seismic assessment of the structure.

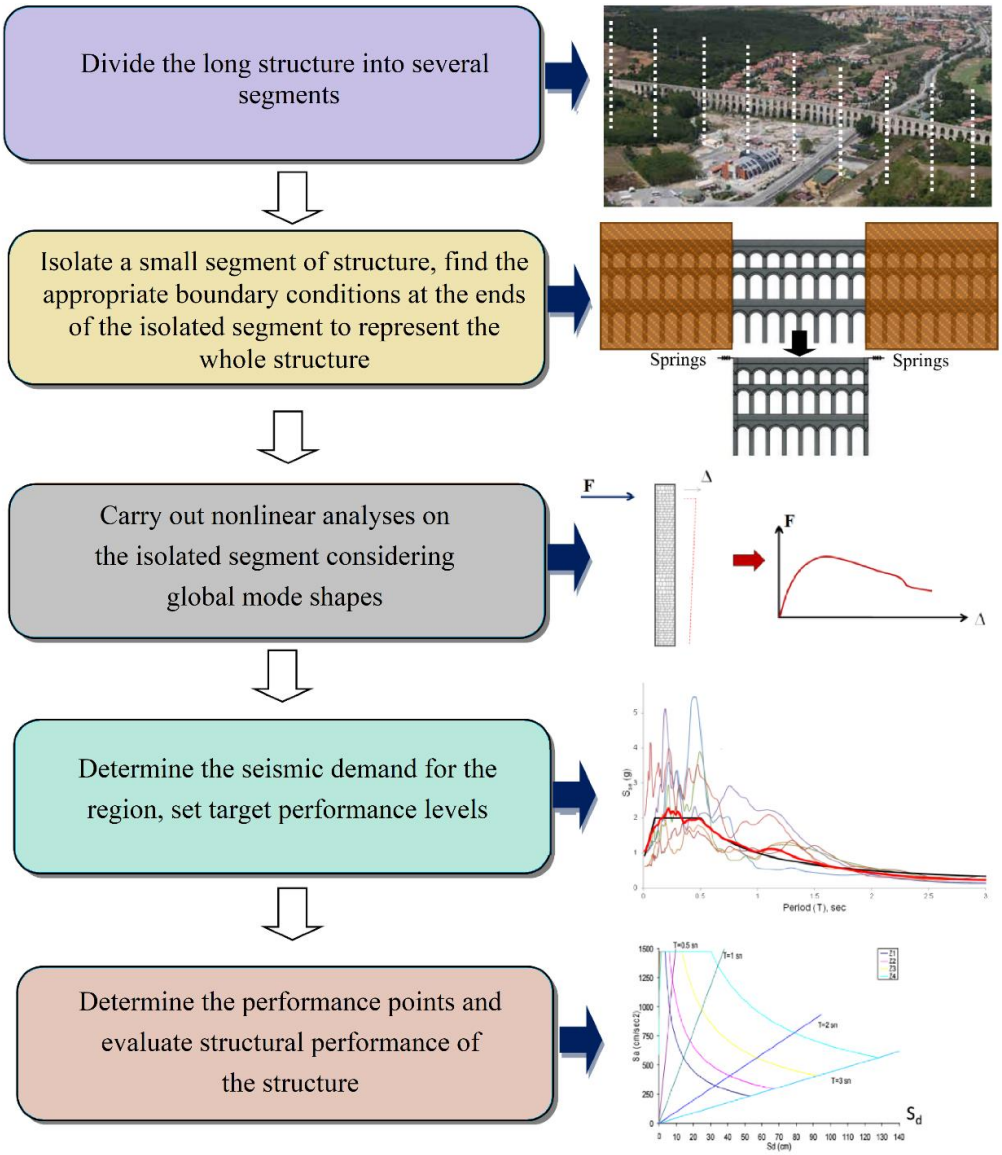

Fig. 2. A layout for performance-based assessment of the long structures.

3. A Case Study: The Valens Aqueduct (Bozdogan Su Kemeri)

3.1. General information

The Valens Aqueduct, which is also known as Bozdogan Su Kemeri, is located in Istanbul, Turkey. The Valens Aqueduct was widely used for supplying water to palaces in history. It stands in the Fatih district of the city and spans the valley between the two hills, which are occupied by Istanbul University and the Fatih Mosque. It was constructed during the late Roman and early Byzantine times. According to historical descriptions, the structure was completed by Emperor Valens (364–378) or Hadrianus (117–138). The aqueduct was later repaired by Emperor Justinian II (576), Konstantinos V (741–775), and Basileios II (1019). During the period of Theodosius II, the aqueduct was used for distributing water to the Baths of Zeus and the Imperial Palace. The structure was restored by Justin II, Basil II and Romanos III. Moreover, during the sovereignty of the Ottoman Empire after 1453, the aqueduct was repaired by Sultan Mehmet II, who was one of the most famous Emperors, and new arches were added to the structure to develop the water supply system. Moreover, the structure was several times restored during the rule of the Ottoman Empire. However, a great part of the Valens Aqueduct was destroyed and only the part located on Atatürk Boulevard has survived (Fig. 3). Although the aqueduct is currently 921 meters long, it was originally 971 meters long, 28.5 meters high and 3.70 meters depth and the aqueduct has 86 different sized arches.

3.2. Performance evaluation

In the performance evaluation, the developed performance-based assessment layout was used and each step in the layout was addressed in detail.

3.2.1. Segmentation and boundary condition

In the scope of the study, the Valens Aqueduct was firstly divided into 125 meters long segments and the segment to be analyzed was isolated. To determine the

stiffness of the springs, two walls were added to the right and left of the isolated segment with the same length as the isolated segment length since it was necessary to express the boundary conditions correctly. The boundary conditions at the ends of the isolated segment can be found by introducing horizontal springs (X and Y directions) at the ends (Fig. 4). Then, the corresponding lateral forces required for a unit displacement of the boundaries for the isolated segment in the X and Y directions were determined by the linear analyses. Finally, these lateral forces were used to determine the lateral stiffness of the springs at the boundaries of the isolated segment. In this model, there are two degrees of freedom spring model was used. In the spring stiffness determination, the force equilibrium equations, Eqs. (1) and (2) were used as follows.

Fig. 3. General views of the Valens Aqueduct (images from Google Images).

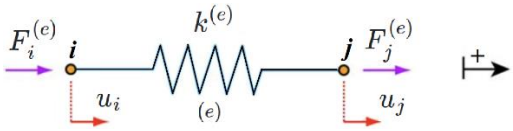

$$k^{(e)}u_i - k^{(e)}u_j = F_i^{(e)} \quad (1)$$

$$-k^{(e)}u_i + k^{(e)}u_j = F_j^{(e)} \quad (2)$$

In matrix form, Eq. (3) was developed.

$$\begin{bmatrix} k^e & -k^e \\ -k^e & k^e \end{bmatrix} \{ \begin{matrix} u_i \\ u_j \end{matrix} \} = \{ \begin{matrix} F_i^{(e)} \\ F_j^{(e)} \end{matrix} \} \quad (3)$$

Since the matrix was symmetric and the order of the matrix was [2×2], the stiffness relation was summarized as Eq. (4).

$$[K^{(e)}]\{u^{(e)}\} = \{F^{(e)}\} \quad (4)$$

where $K^{(e)}$ is the element stiffness matrix, $u^{(e)}$ the nodal displacement vector and $F^{(e)}$ the nodal force vector.

After determining the lateral stiffness of the springs, the structure was discretized with 455210 solid elements with corresponding 1985972 nodes (Fig. 5). In the finite element model (FEM) and finite element analysis (FEA), a general-purpose finite element program, ANSYS Workbench, was used and the isolated segment was numerically modelled with SOLID65 elements, which have eight nodes and three degrees of freedom per node.

In this study, material properties are determined taking into consideration previous studies and general assumptions are made because of the complexity involved in the determination of the material properties (Table 1). In this study, Drucker-Prager Strength Piecewise nonlinear criteria were considered for the nonlinear behavior of the masonry material (Table 2).

Table 1. Mechanical properties of the material.

Property	Value
Density	2300 kg/m³
Young's Modulus	3E+10 Pa
Poisson's Ratio	0,18
Bulk Modulus	1.5625E+10 Pa
Shear Modulus	1.2712E+10 Pa
Max. Tensile Pressure	-4E+6 Pa
Fracture Energy Gf	100 Jm²

Table 2. Drucker Prager strength data.

Pressure (Pa)	Yield Strength (Pa)
0	1E+7
1.5E7	4E+7
5E+7	4.4E+7

Fig. 4. Dividing the structure into segments.

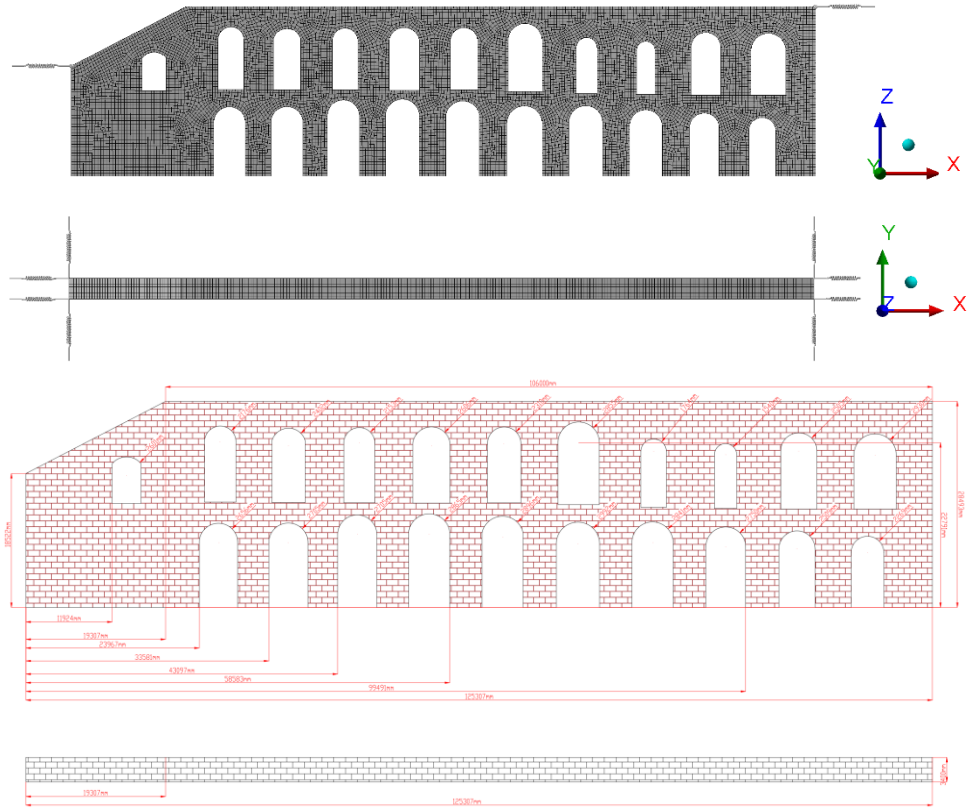

Fig. 5. Numerical model and dimensions of the aqueduct.

3.2.2. Eigenvalue analysis and mode shapes

Modal analysis was performed to determine the dynamic characteristics and seismic behavior of the structure. The modal analysis was conducted including 30 modes and the mass participation ratio in the 30th mode was above 90% in the X and Y directions. The corresponding periods and mass participation ratios obtained with the modal analysis are summarized in Table 3 and the first eight mode shapes of the structure are given in Fig. 6. According to the findings, the first mode and seventh mode were global modes. These global modes constituted an effective mass ratio of more than 71% and 51% in the X and Y directions, respectively. Therefore, in the pushover analysis, the global modes were taken into account and the incremental static analyses in the X and Y directions were performed according to the displacement form in these modes.

3.2.3. Nonlinear static analysis (pushover analysis)

The seismic performance of the structure was investigated through pushover analysis conducted on the finite element model in the X and Y directions. The nonlinear static analysis was made using an incremental-iterative procedure and the analysis procedure adopted in the FEMA 440 and EC-8. To fully define the behaviour in the global modes, the deformation curves of these modes were determined and pushover analysis was performed using these curves (Fig. 7).

Table 3. Frequencies and modal mass participation.

Mode Shape	Frequency (Hz)	Mass Participation Ratios		
		X	Y	Z
Mode 1	2.1878	0.549346E-06	0.509644	0.114848E-10
Mode 2	2.9761	0.124616E-04	0.853842E-03	0.944468E-09
Mode 3	4.3135	0.420495E-07	0.747278E-01	0.102603E-08
Mode 4	5.9585	0.997740E-04	0.803896E-03	0.177276E-07
Mode 5	7.8042	0.947385E-04	0.412953E-01	0.419455E-07
Mode 6	9.8483	0.154870E-01	0.545925E-03	0.619239E-05
Mode 7	10.015	0.713360	0.172893E-03	0.268338E-03
Mode 8	12.111	0.767665E-03	0.714442E-01	0.299998E-06

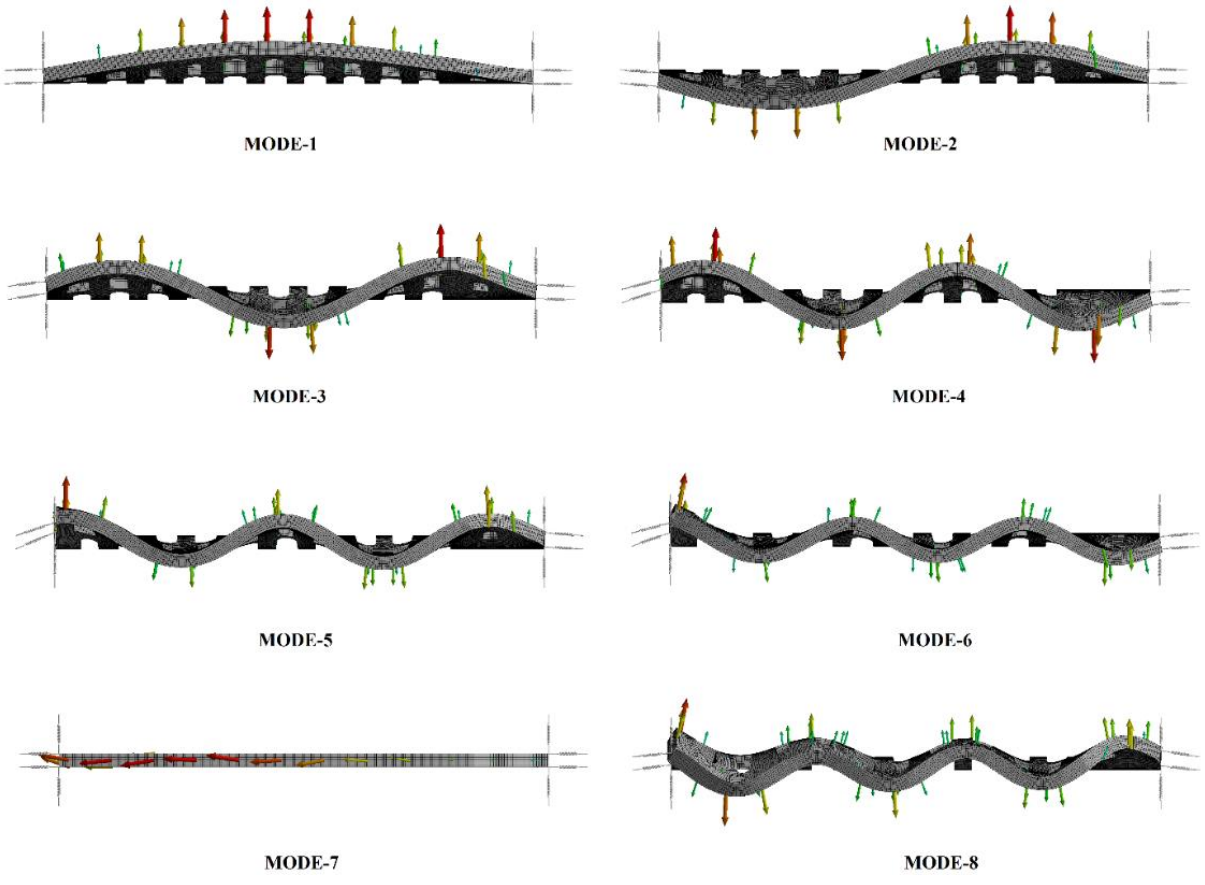

Fig. 6. The first eight mode shapes.

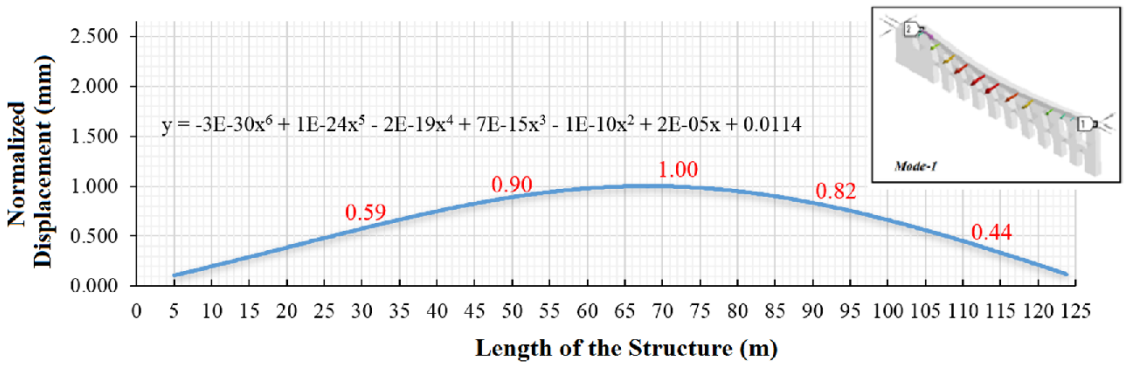

Fig. 7. (continued)

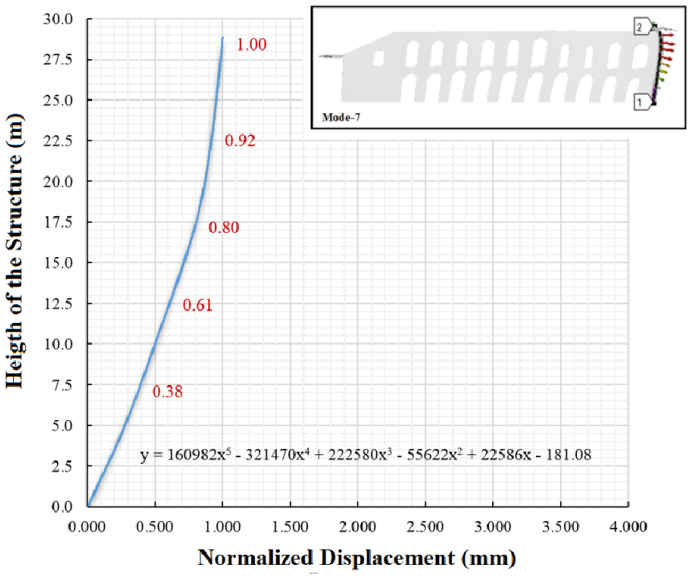

Fig. 7. Normalized displacement pattern obtained from the first and seventh modes.

Based on FEMA 440, in the second phase, the capacity of the structure was determined. The capacity (pushover) curves are plotted in terms of base shear and top displacement. The pushover curve was converted into a modal capacity spectrum by point-by-point conversion of the capacity curve to modal spectral coordinates. Pushover analyses were performed using normalized displacement patterns. In the pushover analysis in the X and Y directions, the equations of the normalized displacement pattern were determined, and incremental static analyses were performed by using these equations. The pushover curves obtained from the pushover analysis in the X and Y directions are presented in Fig. 8a and Fig. 8b, respectively. Then, by using Eqs. (5) and (6) the pushover curves converted to modal capacity curves (Fig. 8c, 8d).

$$a_1^{(i)} = \frac{V_{x1}^{(i)}}{M_{x1}} \tag{5}$$

$$d_1^{(i)} = \frac{U_{xN1}^{(i)}}{\Phi_{xN1}\Gamma_{x1}} \tag{6}$$

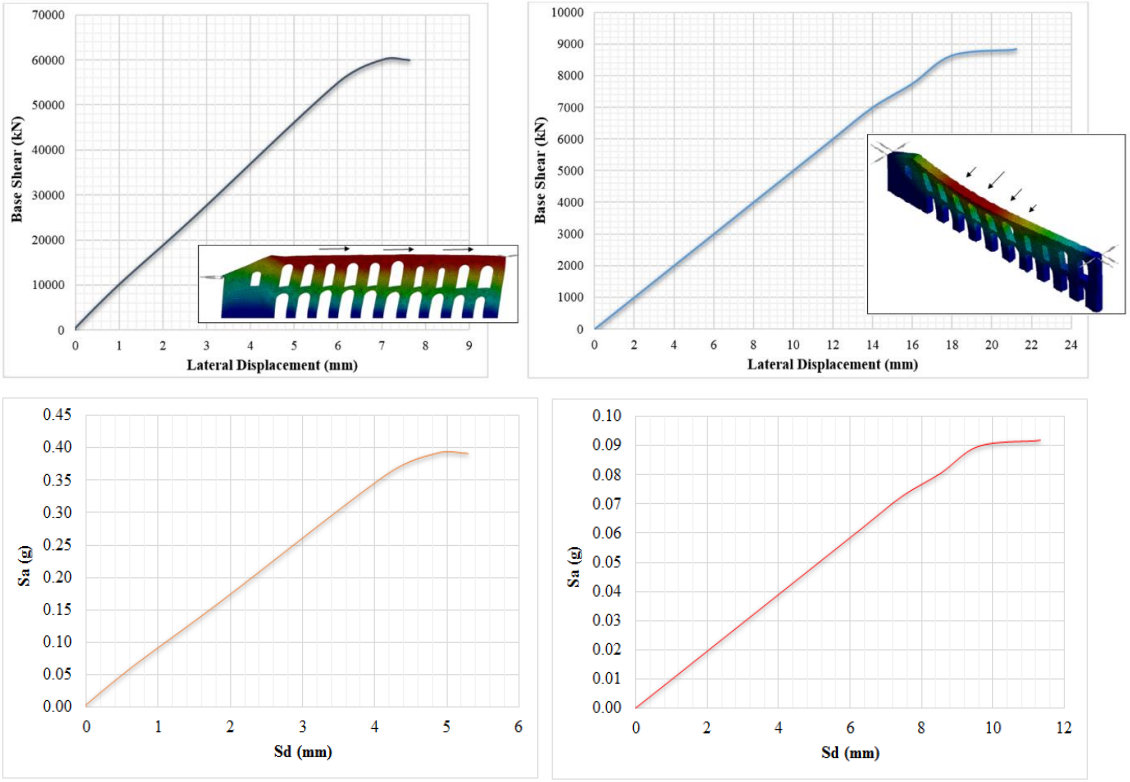

Fig. 8. (a) Pushover curve in the X direction; (b) Pushover curve in the Y direction; (c) Modal capacity curve in the X direction; (d) Modal capacity curve in the Y direction.

3.2.4. Seismic demand

In the seismic demands, two sets of a three-level uniform hazard spectrum; namely, EQ-1, EQ-2, and EQ-3 were constructed using the Turkish Building Earthquake Code-2018 (TBEC, 2018). EQ-1, EQ-2, and EQ-3 for both specifications correspond to the earthquake ground motions with 50%, 10%, and 2% probability of exceedances. EQ-1, EQ-2, and EQ-3 seismic hazard levels were determined using the 5% damped spectral response accelerations at a short period (S_S) and at a period of one second (S_1) are determined for the reference soil type B. The 5% damped spectral response accelerations for short periods (S_S) and at one-second (S_1) for Class B Soil were determined using the site coefficients F_a and F_v. S_S and S_1 were determined as 0.62, 1.19, 1.80 and 0.23, 0.58, 1.02 for EQ-1, EQ-2, and EQ-3 seismic hazard levels, respectively, according to TBEC (2018). F_a and F_v were taken to be 1.0 for EQ-1, EQ-2, and EQ-3 seismic hazard levels, respectively. Both specifications resulted in quite different response spectra in terms of spectral accelerations. Fig. 9a shows the uniform hazard spectra corresponding to these two sets of three-level uniform hazard spectrum. For performance evaluation of the structure, EQ-2 obtained from TBEC (2018) was used as seismic demand due to it is having higher spectral acceleration values at short period region. Then, the response spectrum curve was converted to the demand spectrum by using Eq. (7).

$$S_{ai} = w^2 S_{di} \tag{7}$$

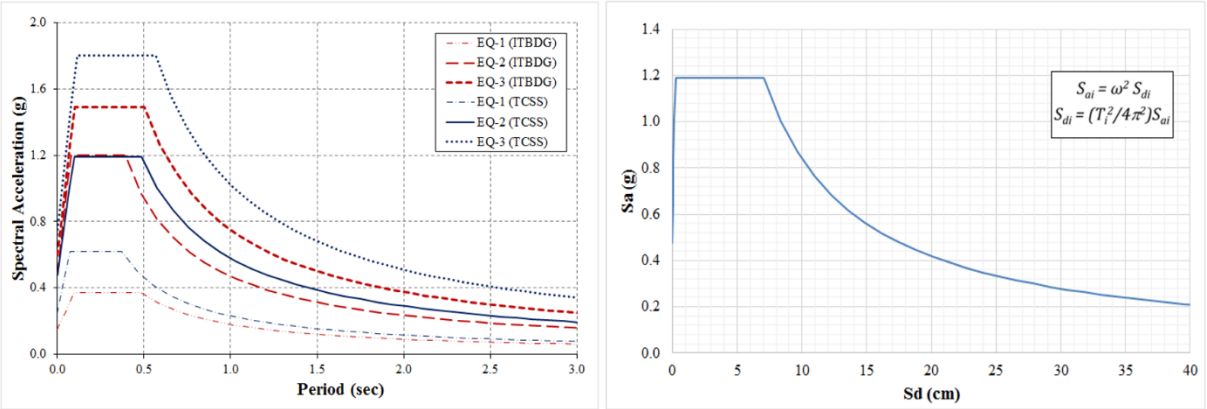

Fig. 9. a) Uniform hazard spectra for the selected seismic hazard levels; (b) Conversion of response spectrum to demand spectrum curve.

3.2.5. Performance evaluation

After the pushover curves were obtained, the coordinate systems were changed to the modal spectrum curves. Then, the modal spectrum curves and seismic demand curves were combined in the same coordinate systems to determine performance points (target displacements) that represent the seismic performance (Fig. 10). Based on the nonlinear static analysis, the target displacement was 10.02 cm in the X direction (in-plane), it was 28.82 cm in the Y direction (out of plane). Top displacements were calculated by using Eq. (8) after the performance points were determined. Top displacements in the X and Y directions are 18.77 mm and 41.58 mm, respectively.

$$u_{xN1}^{(p)} = \Phi_{xN1}\Gamma_{x1}d_1^{(p)} \tag{8}$$

After obtaining the lateral displacement, the drift ratios were determined, and the performance of the structure was evaluated by using the acceptance criteria for URM walls and piers in the current specifications and codes (Table 4). The drift ratio in the X direction (in-plane) was 0.06% while the drift ratio in the Y direction (out-of-plane) was 0.145%.

According to the acceptance criteria, the responses of the Y direction slightly exceeded the immediate occupancy (IO) performance level while the responses of the X-direction remained below the immediate occupancy (IO) performance level. Therefore, it can be said that the performance of the Valens Aqueduct in Istanbul, Turkey is quite good for considered seismic demand. Moreover, as can be seen from Figs. 8a and 8b, it was not possible to laterally push the aqueduct up to these levels of lateral displacements in both directions. The main reason for this was the brittle behavior of the structure. This brittle nature of this masonry structure caused damage during past earthquakes.

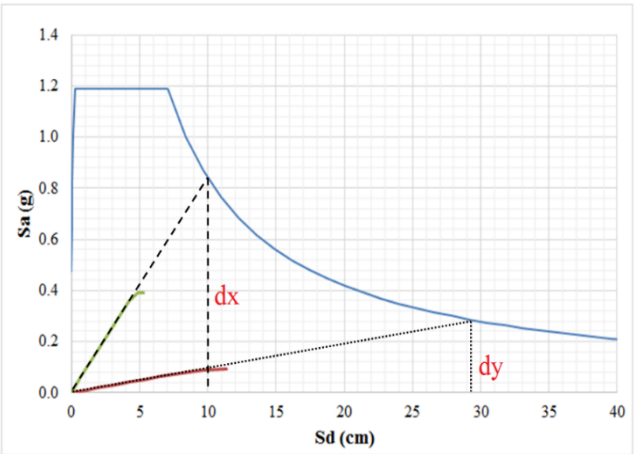

Fig. 10. Performance evaluation.

Table 4. Acceptance criteria for URM walls and piers.

		Primary Members			Secondary Members	
	Limiting Behavioral Mode	Immediate Occupancy (I0) (%)	Life Safety (LS) (%)	Collapse Prevention (CP) (%)	Life Safety (LS) (%)	Collapse Prevention (CP) (%)
FEMA 356 & FEMA 274	Bed-Joint Sliding	0.1	0.3	0.4	0.6	0.8
	Rocking	0.1	0.3 h_{eff}/L	0.4 h_{eff}/L	0.6 h_{eff}/L	0.8 h_{eff}/L
ASCE 41	Rocking	0.1	0.3 h_{eff}/L	0.4 h_{eff}/L	0.6 h_{eff}/L	0.8 h_{eff}/L

h_{eff} = Height to resultant of lateral force

L = Height of wall or pier

4. Conclusions

Masonry aqueducts have been considered to be one of the crucial components of water supply systems throughout history. They are protected with convenient restoration methods and suitable construction materials. The ancient Valens aqueduct studied in this paper was destroyed during past earthquakes and repaired many times in the past. Aqueducts as part of their design have extremely low out-of-plane stiffness compared to the in-plane stiffness. In this study, a practical approach was proposed to assess the structural performance of long historical structures such as aqueducts. This study mainly focused on the numerical modeling and seismic performance of the Valens Aqueduct. A 3D solid numerical model of the structure was constructed and then, the structure was evaluated by the linear and nonlinear analyses. The main outcomes and recommendations obtained from this study are summarized as follows:

- It is not possible to laterally push such brittle structures up to the target displacement when subject to strong earthquake ground motion. The structural behavior is inherently brittle and the structure loses its stability once it starts yielding.
- The past structural damage is consistent with the nonlinear static (pushover) analyses results.
- Since aqueducts are long structures, simple numerical models are needed to understand their structural behavior, because it is almost impossible to model the whole structure. A simple model is proposed in this study. The proposed model is based on isolating a small segment of the structure by introducing linear equivalent springs.
- Long historical masonry structures have a lack of ductility, which is vital from surviving strong earthquake ground motions. Retrofitting schemes for these types of structures should focus on either providing additional lateral strength or ductility.
- Understanding the structural behavior of long historical structures is important in preventing further (progressive) damage and improving their seismic performance.

Acknowledgements

The author would like to thank Prof. Dr. Bulent Akbas for his assistance with the study.

Funding

The author received no financial support for the research, authorship, and/or publication of this manuscript.

Conflict of Interest

The author declared no potential conflicts of interest with respect to the research, authorship, and/or publication of this manuscript.

References

ASCE41-17 (2017). Seismic Evaluation and retrofit of existing buildings, American Society of Civil Engineers. ASCE Standard, ASCE/SEI, 41-17.

Brandonisio G, Lucibello G, Mele E, De Luca A (2013). Damage and performance evaluation of masonry churches in the 2009 L'Aquila Earthquake. *Engineering Failure Analysis*, 34, 693-714.

Cakir F (2021). Tarihi yapıların deprem performansının belirlenmesi için basitleştirilmiş bir yöntem: Kaya Çelebi Cami örneği. *Gazi University Journal of Engineering and Architecture*, 36(3), 1643-1656. (in Turkish)

Cakir F, Uckan E, Shen J, Seker BS, Akbas B (2015). Seismic damage evaluation of historical structures during Van Earthquake, October 23, 2011. *Engineering Failure Analysis*, 58, 249-266.

Dogangun A, Sezen H (2012). Seismic vulnerability and preservation of historical masonry monumental structures. *Earthquake and Structures*, 3(1), 83-95.

EC8-3 (2005). Eurocode 8. 2005. Design of structures for earthquake resistance—part 3: assessment and retrofitting of buildings. EN 1998–3, CEN.

FEMA 440 (2005). Improvement of Nonlinear Static. Seismic Analysis Procedures. Federal Emergency Management Agency (FEMA). Department of Homeland Security (DHS), Washington, D.C.

FEMA 445 (2006). Next-generation performance-based Seismic Design Guidelines, Program Plan for new and existing buildings. Federal Emergency Management Agency (FEMA), Department of Homeland Security (DHS), Washington, D.C.

FEMA P-58 (2018). Seismic Performance Assessment of buildings, volume 1-methodolgy, second edition, Fema P-58-1. Federal Emergency Management Agency (FEMA), Department of Homeland Security (DHS), Washington, D.C.

Gençer F, Hamamcıoğlu-Turan M, Aktaş E (2020). Investigation of in-plane and out-of-plane wall behavior related to lateral loading depending on wall profiles and opening types in Hellenistic Towers. *Gazi University Journal of Engineering and Architecture*, 35(1), 241-253.

Korkmaz M, Ozdemir MA, Kavali E, Cakir F (2018). Performance-based assessment of multi-story unreinforced masonry buildings: The case of historical khatib school in Erzurum, Turkey. *Engineering Failure Analysis*, 94, 195–213.

Lagomarsino S, Cattari S (2015). PERPETUATE guidelines for seismic performance-based assessment of cultural heritage masonry structures. *Bulletin of Earhtquake Engineering*, 13, 13-47.

Lagomarsino S, Modaressi H, Pitilakis K, Bosjlikov V, Calderini C, D'Ayala D, Benouar D, Cattari S (2010). PERPETUATE project: the proposal of a performance based approach to earthquake protection of cultural heritage. *Advanced Material Research*, 133–134, 1119–1124.

Lagomarsino S, Ottonelli D, Cattari S (2019). Performance-based assessment of Masonry Churches: Application to San Clemente Abbey in Castiglione A Casauria (Italy). *Numerical Modeling of Masonry and Historical Structures*, 55–89.

Milani G, Shehu R, Valente M (2017). Seismic performance assessment of three masonry churches through Fe simulations. *AIP Conference Proceedings*, 1863, 450014.

PERPETUATE (2010). Classification of the cultural heritage assets, description of the target performances and identification of damage measures, deliverable D4, performance-based approach to earthquake protection of cultural heritage in European and Mediterranean countries, FP7—Theme ENV.2009.3.2.1.1-Environment, Grant agreement no: 244229, DELIVERABLE D4, June 30, 2010.

Preciado A, Orduna A, Bartoli G, Budelmann H (2015). Façade seismic failure simulation of an old cathedral in Colima Mexico by 3D limit analysis and nonlinear finite element method. *Engineering Failure Analysis*, 49, 20-30.

TBEC (2018). Turkish Building Earthquake Code. Disaster and Emergency Management Presidency (AFAD), March 18, 2018, Ankara.

Challenge Journal of Structural Mechanics

Research Article

Modification of Schmertmann-Hartman-Brown method to estimate immediate (elastic) settlement of shallow foundations

Mustafa Aytekin [a,*]

[a] *Department of Civil Engineering, University of Bahrain, 32038 Isa Town, Kingdom of Bahrain*

ABSTRACT

One of the methods intensively employed in many practical projects to estimate the immediate (elastic) settlement of shallow foundations is the Schmertmann-Hartman-Brown method (1978). In the method, two approaches are given as a function of type of the shallow foundation either a square/circular (axisymmetric condition) or a strip (plain strain condition) foundation. Thus, two sets of equations are provided to estimate the settlements for these types of shallow foundations. If a shallow foundation has a shape of rectangular, some approximations are suggested in the technical literature to estimate the elastic settlement of rectangular based shallow foundations. These approximations are tedious and time consuming. In this study, the Schmertmann – Hartman – Brown method (1978) is modified and only one set of equations used for any type (square, circular, rectangular, and strip) of shallow foundations is introduced. The modified method estimates the immediate settlement as precise as the original form of the method that is more complicated. Also, some hypothetical cases are considered to figure out the effect of width and length/width ratios of foundations on elastic settlement.

ARTICLE INFO

Article history:
Received 23 February 2022
Revised 30 March 2022
Accepted 13 April 2022

Keywords:
Schmertmann-Hartman-Brown method
Elastic (immediate) settlement
Strain influence method
Shallow foundations

1. Introduction

It has been a very important issue to estimate the settlement of foundations for civil engineers. Thus, many researchers have studied the problem to get a reliable solution of it. Terzaghi and Peck (1948) proposed an empirical relationship between the settlement (Se) of a prototype foundation measuring B×B in plan and the settlement of a test plate. Bjerrum and Eggestad (1963) provided the results of 14 sets of load settlement tests. Bazaraa (1967) also provided several field tests results. Both gave correlations of settlements between width (size) of plate used in the tests and size of foundation that would be designed. Jeyapalan and Boehm (1986) and Papadopoulos (1992) summarized the case histories of 79 foundations. DeBeer and Martens (1957) and DeBeer (1965) proposed another formula to estimate the elastic settlement of a foundation. Burland and Burbidge (1985) proposed a method for calculating the elastic settlement of sandy soil using the field standard penetration number N_{60}. The methods in estimation of elastic settlements were summarized (Das et al. 2009)

The Schmertmann-Hartman-Brown method (1978) is commonly used for the estimation of elastic (immediate) settlement of shallow foundations. In the procedure on the estimation of immediate settlement, two approaches are used. One for axisymmetric (square and circular foundations) cases, and the other is for plane strain (strip foundations) condition as seen in Fig. 1. In case of rectangular foundations, there is an approximation in the method by using both axisymmetric and plane strain conditions.

2. Schmertmann-Hartman-Brown Method (1978)

In this method, immediate (or elastic) settlement (S_e) of shallow foundations is calculated by Eq. (1) as seen below.

* *Corresponding author*. Tel.: +973-36936675 ; Fax: +973-17680843 ; E-mail address: maytekin@uob.edu.bh (M. Aytekin)
ISSN: 2149-8024 / DOI: https://doi.org/10.20528/cjsmec.2022.02.003

$$S_e = C_1 C_2 C_3 (q - \sigma'_{zD}) \sum_{i=1}^{n} \frac{\Delta_{zi} I_{zi}}{E_{si}} \quad (1)$$

where

$$C_1 = 1 - 0.5 \left(\frac{\sigma'_{zD}}{q - \sigma'_{zD}}\right) \quad (2)$$

Correction for strain relief due to excavation,

$$C_2 = 1 + 0.2 \left(\frac{t}{0.1}\right) \quad (3)$$

Correction for creep,

$$C_3 = 1.03 - 0.03 \left(\frac{L}{B}\right) \geq 0.73 \quad (4)$$

where q is the gross contact pressure of footing; σ'_{zD} is the effective stress at the base level of footing before the construction; Δz_i is the thickness of soil layer i; I_{zi} is the strain influence factor of layer i; E_{si} is the modulus of elasticity of layer i; B is the width of foundation; L is the length of foundation.

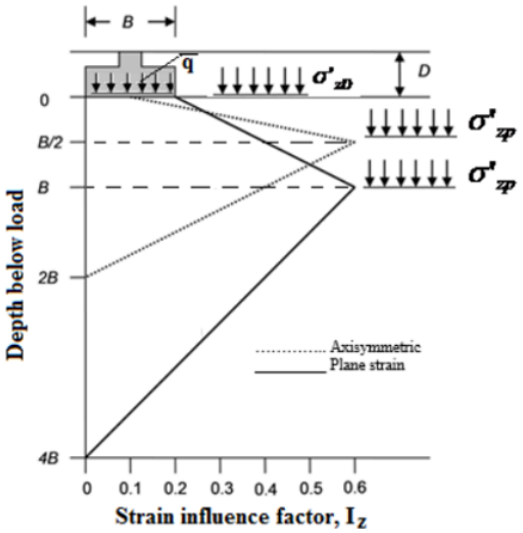

Fig. 1. Variation of stress influence factors for square/circular based (axisymmetric) and strip (plain strain) foundations (Schmertmann et al. 1978).

According to Fig. 1, the exact value of I_{zi} at any depth can be determined as follows; for square and circular footings (L/B=1):

$$I_z = 0.1 + \frac{z}{B}(2I_{zp} - 0.2) \qquad \left(0 \leq z \leq \frac{B}{z}\right) \quad (5)$$

$$I_z = 0.667 I_{zp} + \left(2 - \frac{z}{B}\right) \qquad \left(\frac{B}{z} \leq z \leq 2B\right) \quad (6)$$

For strip (continuous) footings $L/B \geq 10$:

$$I_z = 0.2 + \frac{z}{B}(I_{zp} - 0.2) \qquad (0 \leq z \leq B) \quad (7)$$

$$I_z = 0.333 I_{zp} \left(4 - \frac{z}{B}\right) \qquad (B \leq z \leq 4B) \quad (8)$$

For rectangular footings in which the length is greater than ten times of the width, the plane strain approach is used. In other words, the foundation is considered as a strip foundation. For rectangular foundations in which the length is less than or equal to ten times the width, a linear interpolation between the axisymmetric and plane strain cases is performed, dependent on the length to width ratio. For the rectangular foundations ($1 < L/B \leq 10$):

$$I_z = I_{zp} + 0.111(I_{zc} - I_{zs}) \left(\frac{L}{B} - 1\right) \quad (9)$$

where I_{zp} is the strain influence factor at the depth of z_p (peak value); I_{zc} is the strain influence factor for strip footing that has a width of B; I_{zs} is the strain influence factor for square footing that has a width of B, this value must be at least zero or larger.

As it is seen above, the calculations of strain influence factors are complicated and time consuming. To avoid these problems, the method is modified and a new procedure much simpler than the original Schmertmann et al. (1978) method is introduced in this paper.

3. Modification of the Schmertmann-Hartman-Brown (1978) Method

In this paper, the Schmertmann-Hartman-Brown (1978) method is modified by considering boundary conditions of the square/circular (L/B = 1) and strip ($L/B > 10$) foundations. Equations on the calculation of strain influence factors for any type of shallow foundation such as rectangular, square, circular, strip in Eq. (1) have been re-driven. Thus, the following procedure has been prepared to estimate immediate settlements of any type of shallow foundations. In the modified method, the assumed variation of the strain influence factor is seen in Fig. 2. The user should not be worried about the problem whether it is an axisymmetric or plane strain problem. The data that are needed to be used in the modified method are the size, depth of foundation, load (or bearing pressure), unit weight of soil, number and thickness of soil layers and their modulus of elasticity values under the foundation within the depth of 2B or maximum 4B. The author suggests to users that consider the layers only within the depth of z_{max} that can be calculated by Eq. (18) from the base of foundation as seen in Fig.2.

3.1. Calculation steps of the modified method for any type of shallow foundations:

1. Calculate the followings:

a) Total bearing pressure (contact pressure):

$$q = \frac{P + W_f}{A} \quad (10)$$

where P is the column load; W_f is the weight of footing; A is the base area of footing ($B \cdot L$).

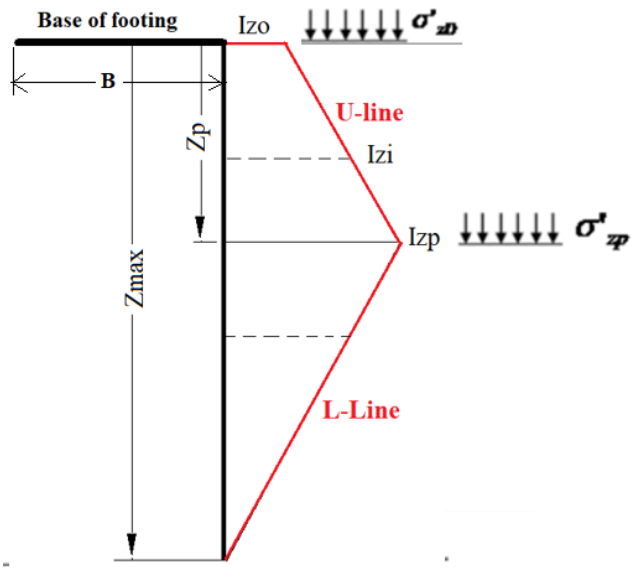

Fig. 2. Variation of the strain influence factor for any type (square, circular, rectangular or strip) of shallow foundations in the modified method.

b) Effective overburden pressure at the base level of foundation before the construction of foundation:

$$\sigma'_{zD} = \gamma D_f - u_D \tag{11}$$

c) Net bearing pressure

$$q_{net} = q - \sigma'_{zD} \tag{12}$$

where u_D is the pore water pressure at the base level of footing; γ is the unit weight of soil above the base-level of foundation; D_f is the depth of foundation from the ground surface.

Up to this point, all the procedure and calculations are same as the original method. After this point, the modifications would take place.

d) Depth of z_p at which the peak of the strain influence factor (I_{zp}) occurs (see Fig. 2). Its value must be $B/2$ and B for square/circular based footings and strip footings, respectively. The following equation can be used for any type of shallow foundations to get the depth at which peak strain influence factor occurs.

$$z_p = \left(\frac{L}{B} - 1\right)\frac{B}{18} + \frac{B}{2} \qquad \frac{B}{2} \le z_p \le B \tag{13}$$

As an alternative, Fig. 3 can be used to get z_p value as follows.

$$z_p = B \cdot C_p \tag{14}$$

where C_p is a coefficient that can be taken from Fig. 3.

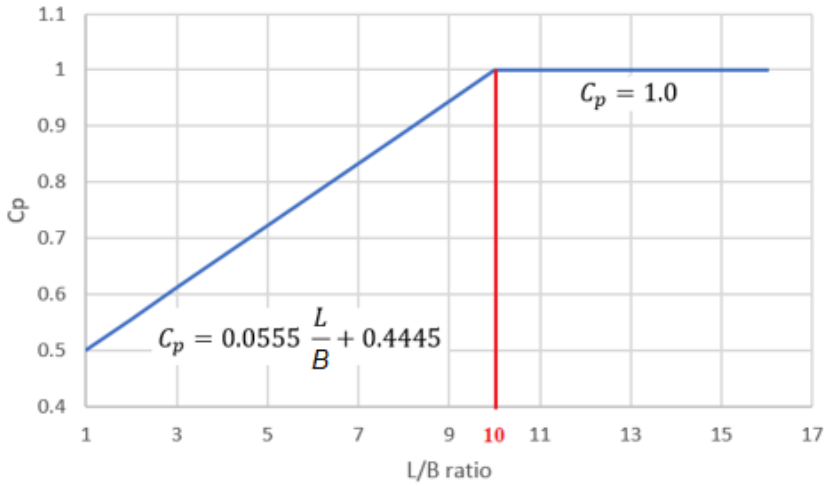

Fig. 3. C_p-coefficient as a function of L/B ratio.

Effective overburden pressure at the depth of z_p at which peak of strain influence factor takes place:

$$\sigma'_{zp} = \sigma'_{zD} + z_p\,\gamma' \tag{15}$$

where γ' is the submerged unit weight of soil if there is ground water otherwise, bulk unit weight of soil.

e) The strain influence factor, I_{zo} (seen in Fig. 2 at the base of any shape of a shallow foundation) can be calculated by Eq. (16). Its value must be between 0.1 and 0.2 (Fig. 4).

$$I_{zo} = \frac{8}{90} + \frac{1}{90}\left(\frac{L}{B}\right) \qquad \left(\frac{L}{B} \le 10\right)$$

$$\left(\text{if } \frac{L}{B} > 10, \text{take } \frac{L}{B} = 10\right) \tag{16}$$

As an alternative, I_{zo} can be taken from Fig. 4 as a function of L/B ratio.

f) The peak value of strain influence factor same as Schmertmann et al. (1978) method:

$$I_{zp} = 0.5 + 0.1\sqrt{\frac{q_{net}}{\sigma'_{zp}}} \tag{17}$$

g) Depth z_{max} at which the strain influence factor would be reduced to zero.

$$z_{\max} = \frac{2}{9}L + \frac{16}{9}B \qquad (2B \le z_{\max} \le 4B)$$

$$(\text{if } z_{\max} > 4B, \text{ take } z_{\max} = 4B) \qquad (18)$$

As an alternative, Fig. 5 can be used to get z_{max} value by Eq. (19).

$$z_{\max} = B \cdot C_m \qquad (19)$$

where C_m is a coefficient that can be taken from Fig. 5.

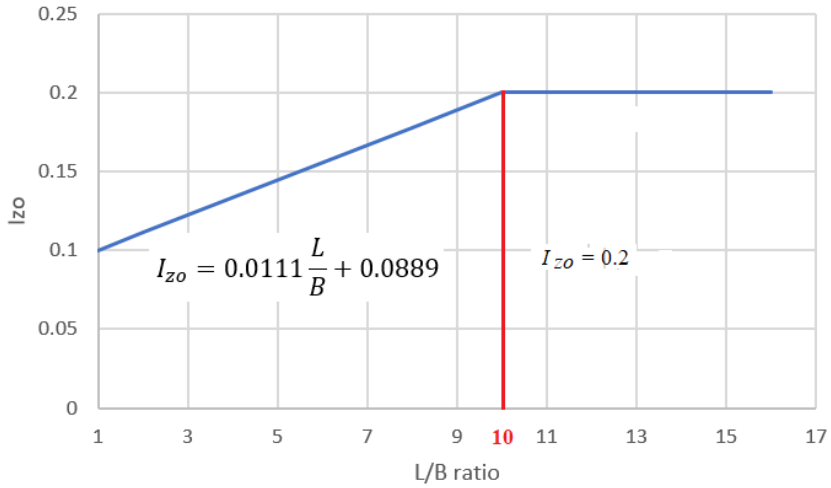

Fig. 4. Variation of I_{zo} as a function of L/B ratio.

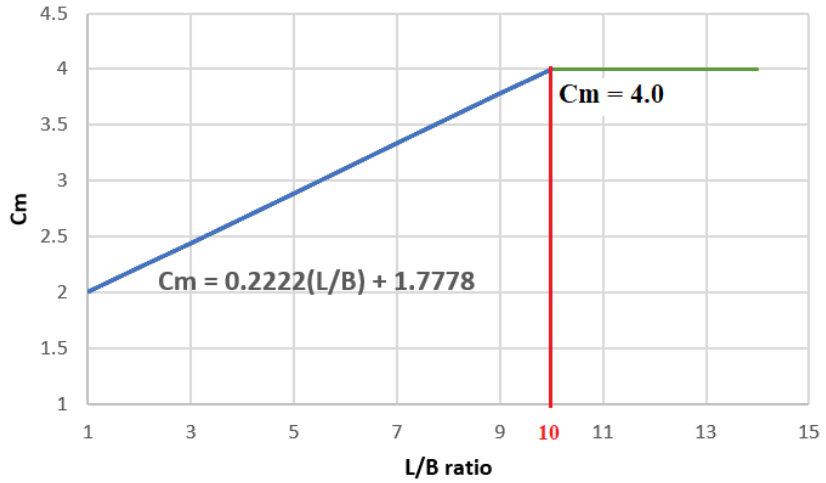

Fig. 5. Coefficient of C_m as a function of L/B ratio.

h) Calculation of I_{zi} values on U-line in Fig. 2 by Eq. (20).

$$I_{zi} = I_{zo} + \left(\frac{I_{zp} - I_{zo}}{z_p}\right) z_i \qquad (0 \le z_i \le z_p) \qquad (20)$$

i) Calculation of I_{zi} values on L-line in Fig. 2 by Eq. (21).

$$I_{zi} = I_{zp} - \left(\frac{I_{zp}}{z_{max} - z_p}\right)(z_i - z_p) \qquad (z_p \le z_i \le z_{max}) \qquad (21)$$

2. Modulus of elasticity is estimated by tip resistance, q_c, of Cone Penetration Test, CPT, if E_s values are not known Eq. (22).

$$E_s = q_c\left(2.389 + 0.111\frac{L}{B}\right) \qquad \left(\frac{L}{B} \le 10\right) \qquad (22)$$

Terzaghi et al. (1996) suggests using the following equation.

$$\frac{E_{s\left(\frac{L}{B}\right)}}{E_{s\left(\frac{L}{B}=1\right)}} = 1 + 0.4 \qquad \log\left[\frac{L}{B}\right] \le 1.4 \qquad (23)$$

where $E_{s(L/B=1)} = 3.5q_c$ and q_c is the cone resistance in CPT (Cone Penetration Test).

Note: If the modulus of elasticity of soil layers are known, no need the estimation by Eqs. (22) or (23).

3. Elastic (immediate) settlement is calculated by Eq. (1), the Schmertmann et al. (1978) method.

4. Hypothetical Cases

Once modification of Schmertmann-Hartman-Brown method was completed, the calculations of the elastic (immediate) settlements became very simple with a simple computer code prepared. Then, the effect of L/B (length/width ratio) and B (width) on elastic settlement is investigated. For the hypothetical cases, the foundation and soil profile seen in Fig. 6 are employed.

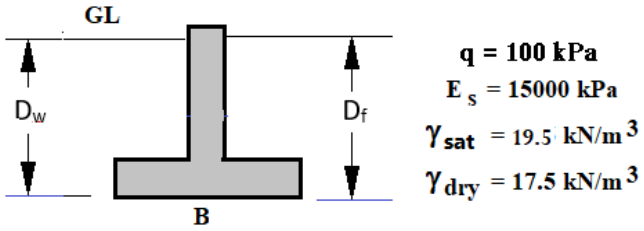

Fig. 6. Soil profile and foundation in hypothetical cases.

The variation of settlements with L/B starting from 1 to 12 (1, 2, 3, 6, 8, 10, 12) for B =1, 3, 5 meters have been estimated by the code and plots are given in Fig. 7. As it is seen in Fig. 7, when L/B is increased, settlement increases too until L/B=10. Then, there is no change on the settlement. Similarly, when B is increased, settlement increases too.

However, once the settlements are normalized as (S_e/B), it has been seen that when L/B increased (S_e/B) increases, and when B is increased, (S_e/B) ratios are decreased as seen in Figs. 8 and 9.

5. Conclusions

From the investigation, following points have been drawn.

- The Schmertmann-Hartman-Brown (1978) method is modified, and a more convenient approach is proposed, so that there would be no worries about the foundation whether it is an axisymmetric problem or a plain strain problem. Also, only two equations would be employed to calculate the strain influence values in place of five equations in the original method.
- The settlements increase from L/B = 1 to 10, after that $(L/B > 10)$ no more settlement would occur.
- It has been seen that the settlement/width ratio decreases while the width of footing is increased. In other words, settlement increment is not linear This result shows that angular distortion of footings with larger width (B) would be less than the angular distortion of footings with smaller B.

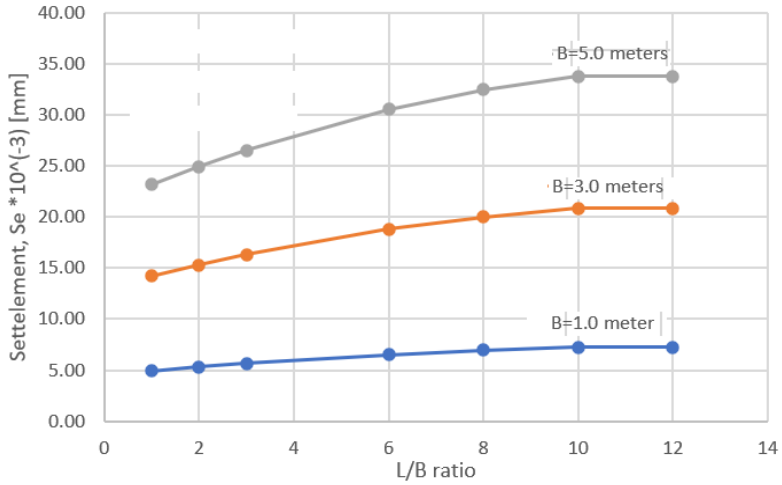

Fig. 7. Settlement/Width ratio versus L/B ratios.

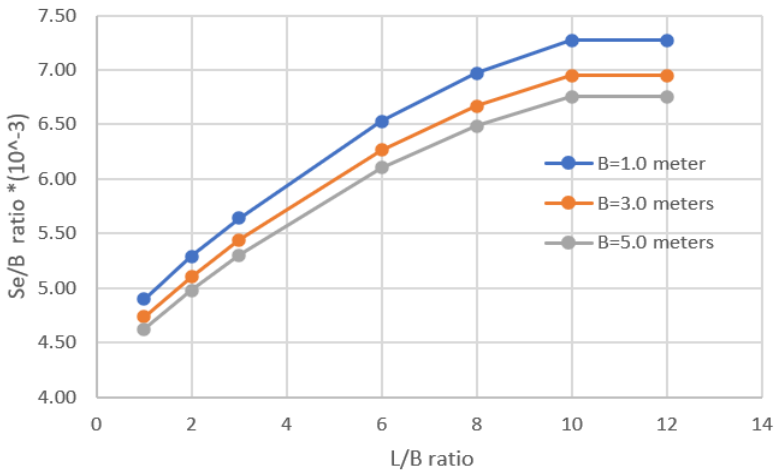

Fig. 8. Settlement/Width ratio versus L/B ratios.

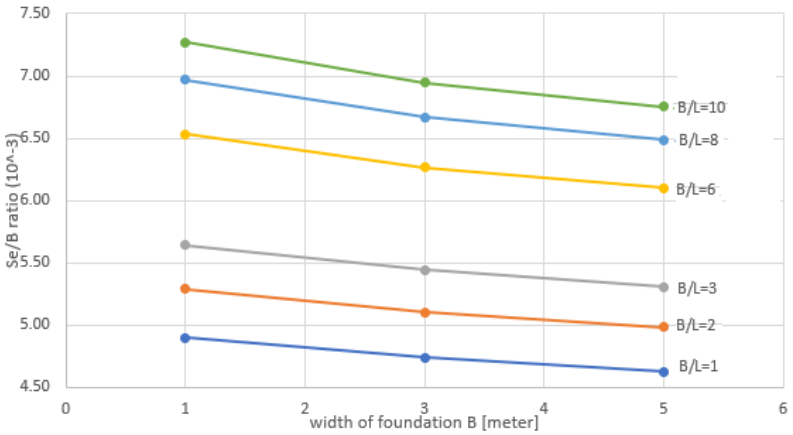

Fig. 9. Settlement/Width ratio versus width (B) of foundation.

Acknowledgements

None declared.

Funding

The author received no financial support for the research, authorship, and/or publication of this manuscript.

Conflict of Interest

The author declared no potential conflicts of interest with respect to the research, authorship, and/or publication of this manuscript.

References

Bazaraa ARSS (1967). Use of the Standard Penetration Test for Estimating Settlements of Shallow Foundations on Sand. *Ph.D. Thesis*, University of Illinois, Champaign-Urbana, Illinois.

Bjerrum L, Eggestad A (1963). Interpretation of load test on sand. *European Conference on Soil Mechanics and Foundation Engineering*, Weisbaden, West Germany, 1, 199.

Burland JB, Burbidge MC (1985). Settlement of foundations on sand and gravel. *Institution of Civil Engineers*, 78(1), 1325-1381.

Das BM, Atalar C, Shin FC (2009). Developments in elastic settlement estimation procedures for shallow foundations on granular soil. *2nd International Conference on New Developments in Soil Mechanics and Geotechnical Engineering*, Near East University, Nicosia, North Cyprus, 9-41.

DeBeer EE (1965). Bearing capacity and settlement of shallow foundations on sand. *Symposium on Bearing Capacity Settlement of Foundations*, Duke University, Durham, NC, 15-33.

DeBeer E, Martens A (1957). Method of computation of an upper limit for the influence of heterogeneity of sand layers in the settlement of bridges. *4th International Conference on Soil Mechanics and Foundation Engineering*, London, 1, 275-281.

Jeyapalan JK, Boehm R (1986). Procedures for predicting settlements in sands. In W.O. Martin (ed.), *Settlements of Shallow Foundations on Cohesionless Soils: Design and Performance*, ASCE, Seattle, 1-22.

Papadopoulos BP (1992). Settlements of shallow foundations on cohesionless soils. *Journal of Geotechnical Engineering, ASCE*, 118(3), 377-393.

Schmertmann JH, Hartman JP, Brown PR (1978). Improved strain influence factor diagrams. *Journal of Geotechnical Engineering Division, ASCE*, 104(8), 1131-1135.

Terzaghi K, Peck RB (1948). Soil Mechanics in Engineering Practice. 1st Edition, John Wiley and Sons, New York.

Terzaghi K, Peck RB, Mesri G (1996). Soil Mechanics in Engineering Practice. 3rd Edition, John Wiley & Sons, New York.

Challenge Journal of Structural Mechanics

Research Article

Evaluating effects of granulated glass on structural and seismic behavior of tall RC structures using experimental tests and 3D modeling

Memduh Karalar [a,*], Murat Çavuşli [a]

[a] *Department of Civil Engineering, Zonguldak Bülent Ecevit University, İncivez, 67100 Zonguldak, Turkey*

ABSTRACT

The use of waste materials for reinforcement of reinforced concrete (RC) structures is of great importance for both environmental cleaning and recycling. In this study, the effects of granulated glass released by factories on the structural behavior of RC structures are examined in detail. Initially, 5 different concretes are produced using 5 different granulated glass percentages. Granulated glass is used instead of aggregate. Different aggregate ratios of granulated glass are taken into account for each sample. 5 different concrete samples are subjected to the slump test and the consistency of the concrete samples is assessed in detail. Then, each concrete sample is subjected to compressive strength tests. It is clearly seen from the compressive strength tests that granulated glass increased the strength of the concrete noticeably. Then, the 31-story reinforced concrete structure is modeled considering the most critical granulated glass ratio. The 1995 Kobe earthquake is utilized for the seismic analyses. Firstly, the RC structure is analyzed for the pure concrete and then, analyses are performed for various granulated glass added cases. According to the analysis results, granulated glass significantly increased the earthquake resistance of reinforced concrete structures. Furthermore, waste granulated glass caused enormous reductions in the weight of the structure. In this study, it is concluded that granulated glass material, which is found in nature as waste, can be used for the construction of RC structures.

ARTICLE INFO

Article history:
Received 11 March 2022
Revised 8 April 2022
Accepted 10 May 2022

Keywords:
Compressive stress
Finite element modeling
Granulated glass
Reinforced concrete structure
Slump test

1. Introduction

Ensuring the earthquake safety of tall reinforced concrete (RC) structures is very important for the safety of the people living in these structures. In the past, many methods have been used to strengthen RC structures and one of these methods is to use additives in the concrete. One of these additives is granulated glass and granulated glass is released from factories as waste material to nature. When the literature is examined, it is seen that granulated glass is rarely not used for earthquake reinforcement of RC structures. For this reason, in this study, the effects of granulated glass on the earthquake safety of tall RC structures are investigated in detail. Many studies have been carried out on the earthquake strengthening of RC structures in the literature. Shen et al. (2021a) examined the seismic behavior of the RC building joints using the basalt fiber-reinforced polymer sheets. Firstly, five various column-beam joints were prepared considering all original specimens. In the experimental loading process, the horizontal displacements and loads applied on the test specimens were monitored, and the cracks were signed at the surface in each cycle. According to experimental tests, it was seen that generally, the seismic behavior of beam-column joints was increased by these five strengthening schemes. For specimen SBC2, better performance of ductility and energy dissipation capacity could be obtained

* *Corresponding author*. Tel.: +90-372-291-2582 ; Fax: +90-372-257-4023 ; E-mail address: memduhkaralar@beun.edu.tr (M. Karalar)
ISSN: 2149-8024 / DOI: https://doi.org/10.20528/cjsmec.2022.02.004

by strengthening the interior beam-column joints with the whole lengths of the beams and column in the practical RC frames. Shen et al. (2021b) assessed the flexure and crack behavior of the RC buildings utilizing fabric reinforced Alkali-Activated Slag matrix. The crack patterns and failure modes of the RC beams with and without strengthening were evaluated in detail. According to experimental tests, the control specimen failed in a typical flexural mode for a ductile concrete beam. Moreover, cracks first appeared in the tensile zone at the mid-span of the beams. The yielding of longitudinal reinforcements subsequently occurred as the deflection increased, followed by the crushing of concrete in the compression zone. Tests showed that specimen B–O–S-A0 exhibits a slight improvement in loading capacity over the control specimen at the yielding stage, followed by a sudden drop in load due to the premature end-debonding at the concrete-matrix interface. Nanda et al. (2020) investigated the effects of metakaolin and Recron 3s fiber on the structural behavior of concrete material. Metakaolin was used as a partial replacement for Portland slag cement (PSC). Compressive strength was examined for separate mixtures prepared from the different % replacement of metakaolin (5%, 10%, and 15%) and fly ash (10%, 20%, and 30%) by weight of cement with a constant 0.2% of Recron 3s fiber. Experimental tests showed that blending of metakaolin, fly ash and Recron 3s fiber enhance the overall mechanical properties of concrete. However, with only metakaolin replacement, the best replacement was found to be 10% by weight of cement and the enhancement of compressive strength, split tensile strength and flexural strength was estimated to be 10.25%, 9.46%, and 12.34% respectively at 28 days curing. Wu et al. (2020) assessed the application of bacterial spores coated by a green inorganic cementitious material for the self-healing of concrete cracks. Firstly, the properties of the biocapsule were analyzed and the effect of its dosage on cement mortar properties was evaluated. Then, crack-healing efficiency and water permeability were evaluated to assess the effectiveness of the biocapsule in crack self-healing. According to experimental tests, the addition of biocapsules at a dosage of 5% of the cement mass led to full healing of 150–550 μm width cracks. Furthermore, it was seen that when the biocapsule dosage was less than 5%, the strength of concrete specimens increased with an increase in dosage. Tang et al. (2020) examined the seismic behavior of the fly ash/slag-based geopolymeric recycled aggregate concrete under both quasi-static and dynamic loadings. The experimental tests showed that the compressive properties of geopolymeric recycled aggregate concrete exhibit a strong strain rate dependency. Besides, although the recycled aggregate replacement decreases the quasi-static compressive strength, it exhibits a slight effect on the compressive strength at high strain rates. Then, empirical dynamic increase factor formula for compressive strength of geopolymeric recycled aggregate concrete are proposed, in which the dynamic increase factor increases approximately linearly with the strain rate in a logarithmic manner. Ramdani et al. (2019) assessed the structural properties of concrete material with waste rubber aggregate, glass powder, and silica sand powder. Various rubber aggregate ratios (10%, 20%, 40%, and 60%) were utilized to replace crushed sand in concrete mixes. Moreover, glass powder and natural sand powder were considered to replace 15% of the cement weight. Nine different forms of concrete with separate wastes and with the combination of them were designed and prepared. The experimental results showed that the strength increased with the incorporation of glass powder and rubber aggregates, especially with 10% and 20% Rubber aggregate contents. Güneyisi et al. (2019) investigated the fresh and rheological properties of glass fiber reinforced self-compacting concrete with nano-silica and fly ash blended. Fifteen mixtures of self-compacting concrete fortified by glass fibres with dissimilar quantities of pozzolanic replacement cement were prepared in a constant water-binder ratio of 0.35 and a total binder content of 550 kg/m^3. The results showed that self-compacting concrete with replacement of 2% and 4% NS and maximum amount of GF achieved the lower rate of workability enhancement. Zhang et al. (2019) evaluated the mechanical behavior of seawater sea-sand recycled coarse aggregate concrete columns under axial compressive loading. The experimental results showed that the seawater-sea-sand-based concrete column behaves similarly to conventional natural aggregate concrete when the shell content in sea-sand equals 2.31%. Xie et al. (2018) examined the effects of the addition of silica fume and rubber particles on the compressive behavior of recycled aggregate concrete with steel fibres. The silica fume and rubber contents were the main test parameters. It was seen that rubberized steel-fiber recycled aggregate concrete with 100% recycled coarse aggregate, 10% silica fume, and 5% rubber is a more environmentally friendly alternative to normal concrete for use in the compression member of concrete structures. Dash and Patro (2018) assessed the effects of water-cooled ferrochrome slag as fine aggregate on the properties of concrete. Compressive strength tests, splitting tensile strength tests, flexural strength, and modulus of elasticity tests were conducted on various concrete samples containing 0–50% of the water-cooled ferrochrome slag on replacement of equal weight of natural sand. The experimental test results showed that there is a little decrease in strength properties of concrete due to the inclusion of the water-cooled ferrochrome slag but can be used up to 30% with minor scarification of strength. Thorneycroft et al. (2018) evaluated the performance of structural concrete with recycled plastic waste as a partial replacement for sand. The results indicated that replacing 10% sand by volume with recycled plastic is a viable proposition that has the potential to save 820 million tonnes of sand every year. Mohajerani et al. (2017) assessed the practical recycling applications of crushed waste glass in construction materials. According to a review study, it was seen that crushed waste glass has potential use as an aggregate in construction materials. Then, there are many studies about the strengthening of reinforced concrete buildings using waste materials (such as waste granulated glass, industrial lathe wastes) in the literature such as Tamburini et al. (2017), Lynn et al. (2015), Refai et al. (2015), Younis and Pilakoutas (2013), Boukendakdji et al. (2009), Frazão et al. (2019),

El-Sayed (2019), El-Sayed (2021), El-Sayed and Shaheen (2020), El-Sayed et al. (2019a), El-Sayed et al. (2019b). As seen from these studies, the effects of waste granulated glass material on the seismic behavior and strengthening behavior of reinforced concrete structures have not been examined in the past. Thus, this study is of great importance to fill this gap in the literature. In this study, firstly, 5 different ratios of the granulated glass material are used instead of aggregate in concrete material. Concrete samples prepared in the laboratory are subjected to compressive strength tests and the effects of granulated glass utilized in concrete on concrete strength are determined. After the most critical granulated glass ratio is determined, this granulated glass ratio is considered for the concrete material of a 31-story RC structure. Then, reinforced concrete structure with a pure concrete structure and reinforced concrete structure with granulated glass are subjected to earthquake analyses and according to the earthquake analysis results, the effects of granulated glass on the earthquake behavior of reinforced concrete buildings are determined in detail. Experimental and numerical results show whether the granulated glass material left to nature as waste can be used in RC structures.

2. Material and Method

In this study, the effects of granulated glass released as waste material by factories on the seismic behavior of reinforced concrete structures are revealed. When the literature is examined, it is seen that there are very few researchers studying the effects of granulated glass on the earthquake behavior of reinforced concrete structures, and this study aimed to eliminate these deficiencies in the literature. In this study, firstly, concrete samples with 5 different additives are prepared. Granulated glass is used instead of aggregate in concrete samples. After the pure concrete is prepared, concretes with granulated glass are formed by using 5%, 10%, 15%, and 25% rates instead of the aggregate in the concrete. 3 different samples are prepared for each concrete with additives and slump tests are carried out to obtain the consistency of these concretes. Slump tests are performed following the standards and very large consistency differences are observed between the additive concrete and pure concrete. Then, these additive concrete samples are kept in water for 7 days, 14 days, and 28 days. Concrete specimens that reached sufficient hardness are subjected to compressive strength tests. During the compressive strength tests, the dimensions of the samples, the test starting speed, and the correction rate are defined to the device. After the pressure tests are performed, the time-dependent strength graphs of each glass powder added to the concrete are acquired. According to the test results, very large strength differences are observed between the additive concretes and pure concrete. Then, a 31-story reinforced concrete structure is modeled by considering the most critical granulated glass ratio. Modeling is performed using SAP2000 software and the finite element method is utilized in the seismic analysis. All the load-bearing elements of the building (beam, column, and floor) are created by considering the original project of the building. A fix boundary condition is defined at the base of the structure. In earthquake analysis, the 1995 Kobe earthquake is used. Furthermore, X, Y, and Z components of each earthquake are taken into account for earthquake analyses. The nonlinear situation is considered in the dynamic analyses. The structure is first analyzed for the case modeled with pure concrete. Then, the structure modeled with granulated glass added concrete is subjected to earthquake analyses. According to the analysis results, it is concluded that the use of granulated glass has positive effects both on the earthquake behavior of reinforced concrete structures and on recycling.

3. Mechanical Properties of Waste Granulated Glass

In developing industrial facilities, a very high increase is seen in industrial wastes due to effects such as the increase in population (Uzun et al. 2018). The storage, disposal, or reuse of these wastes has become an important research topic. Waste glass, like other industrial wastes, is difficult to dissolve and has high recycling costs. On the other hand, the fact that it is rich in silica and that there is a lot of waste around the world makes the waste glass more important. Glass production takes place by cooling high-temperature calcium carbonate, soda ash, and molten silica while solidification takes place without crystallization (Uzun et al. 2018). Worldwide waste is estimated to be 200 million tons in 2004, of which 7% consists of glass products. In 2013, 11.54 million tons of waste glass were generated in the USA alone, and only 27.3% of it was recycled. It is widely used in the reinforcement of many composites such as glass, fiber, and aggregate (Uzun et al. 2018). Many studies have been conducted on the use of glass waste in different ways, such as aggregate in concrete, as a filler, as an alkali-activated binder, and as an additive to cement. Thanks to the pozzolanic feature of waste glass, it allows use in concrete. Some trials have been made as concrete aggregate, but the cracks on the concrete surface have created negativity (Uzun et al. 2018). More positive results were obtained in the studies carried out to use the granulated glass as an additive to the cement by grinding it under 0.005 mm size. Many studies have been carried out to increase strength and durability, especially as a result of using it as an additive to cement. The purpose of using waste granulated glass as an additive to cement is to benefit from the silica it contains. Granulated glass provides additional advantages thanks to its pozzolanic feature (Uzun et al. 2018). Granulated glass reacts with portlandite (Ca(OH)2) formed during cement hydration of amorphous silica (SiO2) in the granulated glass to form calcium silica hydrate (C-S-H) structures. The reactions of the waste granulated glass used are given below (Uzun et al. 2018).

$$SiO_2(s) + Ca_2 + (aq) + 2OH - (aq) = n1CaO.SiO_2.n2H_2O(s) \quad (1)$$

Fig. 1. View of granulated glass (Uzun et al. 2018).

4. Preparation of Concrete Samples

In this study, the effects of granulated glass, which is found as waste in nature, on the earthquake behavior of reinforced concrete structures are investigated in detail. For this reason, first of all, waste granulated glass added concrete cube samples are created in the laboratory. In the laboratory, 5 various cube concrete samples are created in detail. Firstly, pure concrete cube samples are generated. To create pure concrete, 10.7 kg cement, 32.2 kg aggregate, 5.2 kg water are used. Then, granulated glass added concretes are produced and 10.7 kg cement, 30.6 kg aggregate, 5.2 kg water, and 1.6 kg granulated glass are utilized to form M1 added to concrete. Furthermore, 10.7 kg cement, 29.02 kg aggregate, 5.2 kg water, and 3.2 kg granulated glass are considered to create M2 added concrete. Then, 10.7 kg cement, 27.4 kg aggregate, 5.2 kg water, and 4.8 kg granulated glass are used to produce M3 added concrete. Finally, 10.7 kg cement, 25.7 kg aggregate, 5.2 kg water, and 6.4 kg granulated glass are taken into account for M4 added to concrete. The materials used in 5 different concrete samples produced in the laboratory are summarized in detail in Table 1. A total of 3 different samples are prepared for each additive concrete (Fig. 2). Fig. 2 shows the view of placing concrete samples with and without additives in the molds. In Fig. 3, the view of the preparation of concrete samples and the mixing of materials in the mixer is shown. A special mixer is used in the laboratory to prepare concrete samples. After preparing 3 different pure concrete, 3 different M1 samples, 3 different M2 samples, 3 different M3 samples, and 3 different M4 samples, the concrete samples are subjected to slump tests. In addition, 3 samples are prepared for each concrete with additives to obtain 7-day, 14-day, and 28-day strengths. The appearance of the slump tests is shown in Fig. 4. According to Fig. 4, slump tests are performed using 2 different methods (Figs. 4a and 4b). Fig. 4c shows how the consistency amounts are measured for concrete samples. In Table 2, 7-day slump test results are presented in detail. According to Table 2, the slump test result obtained for pure concrete is 20 mm. Besides, the amount of slump obtained for M1 concrete is 115 mm. For M2 and M3 concrete samples, 45 mm and 18 mm slump amounts are observed, respectively. Finally, 80 mm slump is acquired for M4 concrete. Moreover, 7-day, 14-day, and 28-day slump test results are shown in Fig. 5 comparatively. According to Fig. 5, it is concluded that the slump obtained for the 7-day concrete samples is greater than the 14-day and 28-day samples. In addition, the lowest slump is obtained for M3 concrete samples for 7-day, 14-day, and 28-day concrete samples. The highest slump is observed for M1 concrete samples. After the prepared concretes are placed in cube samples and subjected to slump tests, the samples are kept in water for 7 days, 14 days, and 28 days (Fig. 6). For this process, a special water pool is used and the water temperature is defined to the device to provide more realistic results. Fig. 7 shows the view of the device used to pressure test concrete samples. Both cube and cylindrical concrete samples can be used in the device used for pressure tests. Furthermore, the dimensions of the samples, correction coefficients, and test speed can be defined in the device during the test. After the test is performed using the device, the results can be printed from the device both with the help of USB and in writing (Fig. 8).

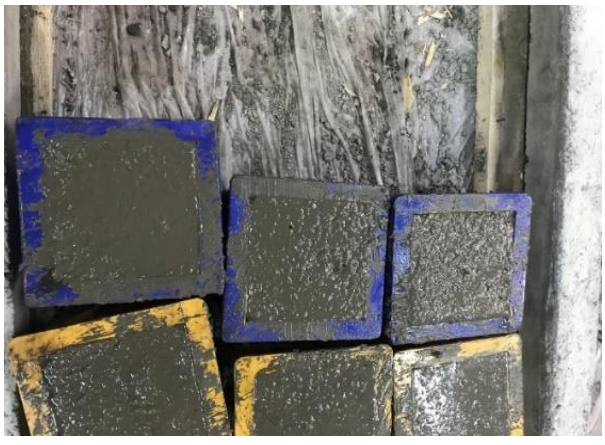

Fig. 2. Preparing concrete molds in the laboratory.

Table 1. Material weights of concrete samples.

Situation	Material	Weight (kg)
Pure Concrete	Cement	10.731
	Aggregate	32.235
	Water	5.250
	Ground Glass	0
M1	Cement	10.731
	Aggregate	30.618
	Water	5.250
	Ground Glass	1.617
M2	Cement	10.731
	Aggregate	29.022
	Water	5.250
	Ground Glass	3.234
M3	Cement	10.731
	Aggregate	27.405
	Water	5.250
	Ground Glass	4.830
M4	Cement	10.731
	Aggregate	25.788
	Water	5.250
	Ground Glass	6.447

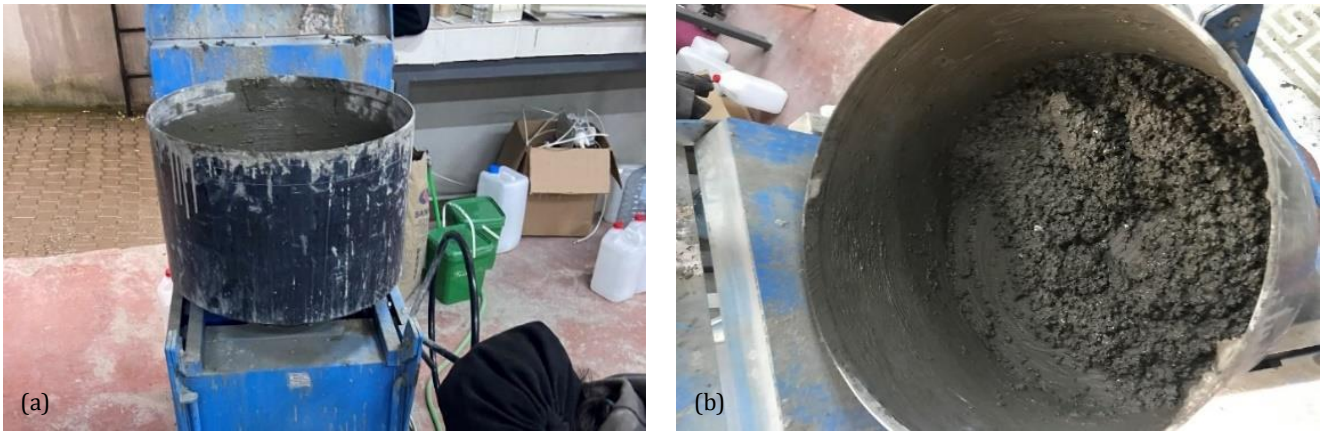

Fig. 3. Mixing of materials for creating concrete sample.

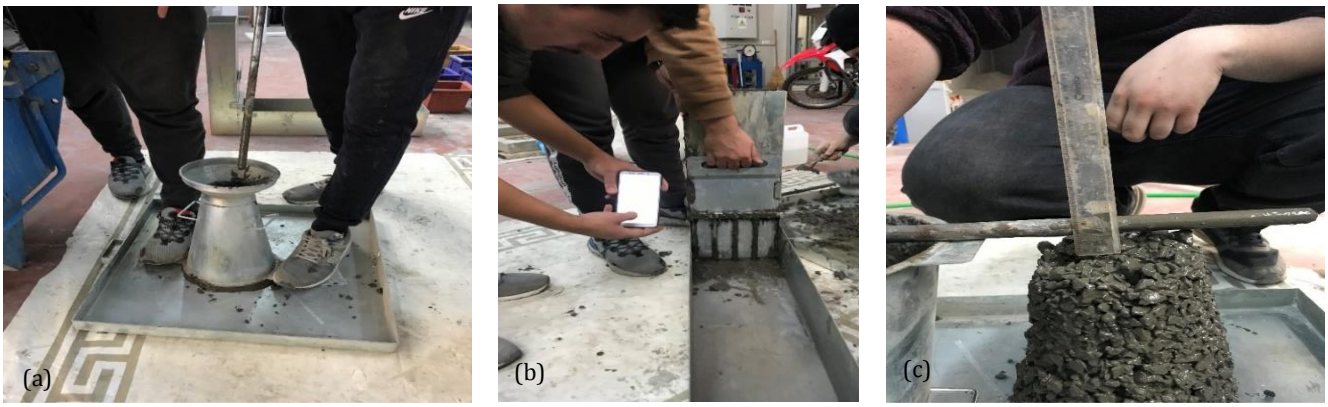

Fig. 4. Views of various slump tests.

Table 2. Slump test results of concrete samples.

Mix	Ground Glass (%)	Slump Value (mm)
Pure Concrete	0	20
M1	5	115
M2	10	45
M3	15	18
M4	20	80

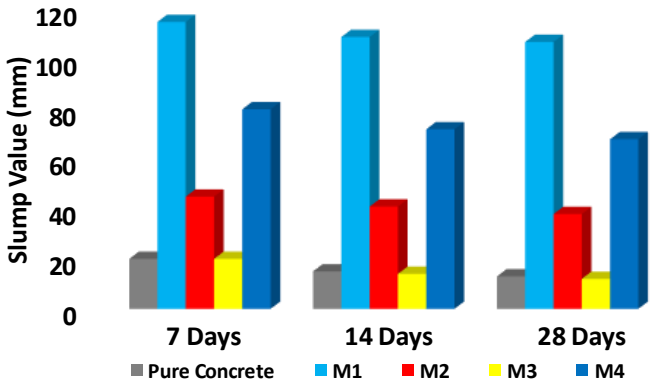

Fig. 5. Detailed slump test results.

Fig. 6. Keeping the concrete samples in the water pool.

Fig. 7. General view of the prepared concrete samples.

Fig. 8. Using the compressive strength device.

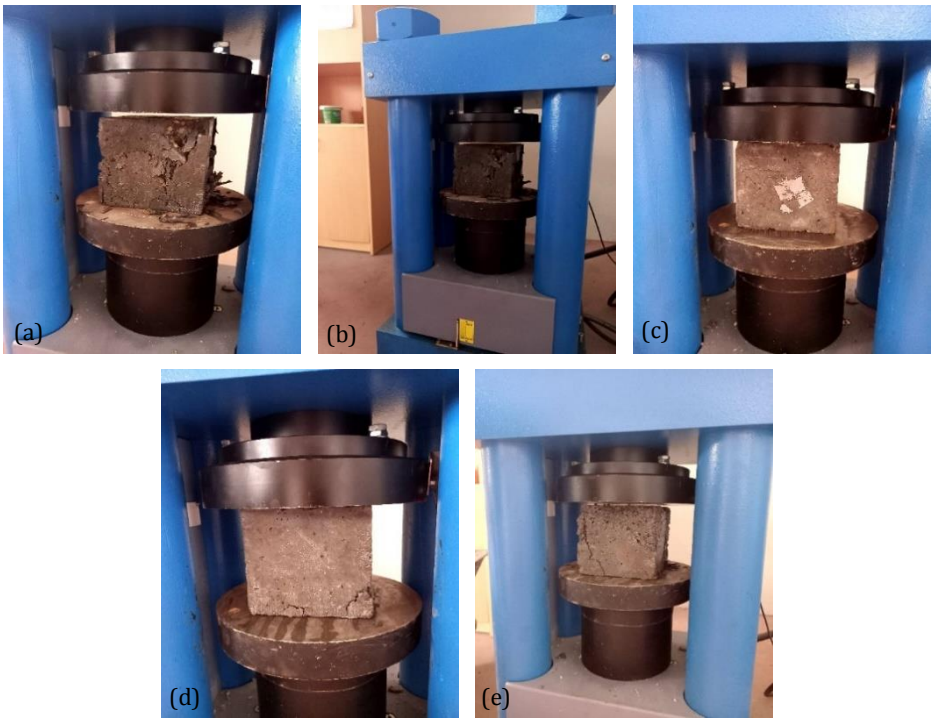

Fig. 9. View of concrete samples during compressive strength test:
a) Pure concrete; b) M1 sample; c) M2 sample; d) M3 sample; e) M4 sample.

Fig. 10. View of all concrete samples subjected to compressive strength test (for 7 days).

Fig. 9 shows the appearance of 5 different mixed concrete samples subjected to pressure tests. During the experiments, protective clothing was worn to protect human safety. According to the results of the pressure test, it is seen that the granulated glass additive changes the strength of the concrete. Fig. 9a shows the view of the pressure test for pure concrete. According to Fig. 9a, significant cracks and damages occurred in the pure concrete during the test. Fig. 9b shows the view of the pressure test performed for the M1 sample. According to Fig. 9b, it is seen that the cracks occurring in 5% granulated glass added concrete is more than in pure concrete. In addition, the concrete test results acquired for the M2 sample are shown in Fig. 9c. When Figs. 9b and 9c are compared with each other, it is openly seen that the cracks that took place in the concrete sample are less for M2 concrete. In Figs. 9d and 9e, the compression test results obtained for the M3 and M4 samples are shown and it is observed that the concrete cracks obtained for the M3 and M4 samples are more than the M2 sample. In Fig. 10, the appearance of the 7-day concrete samples subjected to the compressive strength test is shown. When Fig. 10 is examined in detail, it is clear that the largest cracks occurred for pure concrete. Furthermore, it is observed that the smallest concrete cracks are gained for the M2 sample. In Table 3, the test results of concrete samples subjected to the compressive strength test are shown in detail. When Table 3 is assessed, the maximum carrying load value obtained for 3 different pure concrete samples is 428 kN. The smallest carrying load value is 369 kN. Moreover, Table 3 shows the compressive strength test results acquired for the M1 sample and the largest carrying load value obtained for 3 different M1 samples is 478 kN. The compressive test results obtained for the M2 sample are shown. The smallest and largest carrying load values acquired for 3 different M2 samples are 486 kN and 513 kN, respectively. As the compressive test results for M3 and M4 samples are evaluated, it is understood that the maximum carrying load value obtained for the M4 sample is much smaller than that of the M3 sample. When the 7-day concrete samples are compared with each other, it is concluded that the concrete sample with the highest strength is the M3 sample. In addition, it is observed that the concrete sample with the smallest strength is the M4 sample. It is clear from these results that 15% granulated glass added concrete is more durable than pure concrete, and as 5%, 10%, 15%, and 20% granulated glass added rates are compared, it is concluded that the most critical additive rate increasing the strength of pure concrete is 15% granulated glass additive ratio.

Table 3. Compressive strength results for 5 various concrete samples.

		7 Days (kN)	Average	14 Days (kN)	Average	28 Days (kN)	Average
Pure Concrete	Sample 1	418	395	429	424	612	579
	Sample 2	402		434		543	
	Sample 3	367		411		582	
M1 Concrete	Sample 1	482	454	581	529	782	758
	Sample 2	457		517		771	
	Sample 3	423		491		723	
M2 Concrete	Sample 1	515	492	747	723	903	879
	Sample 2	484		732		884	
	Sample 3	478		691		852	
M3 Concrete	Sample 1	431	400	877	857	1172	1050
	Sample 2	401		851		1052	
	Sample 3	368		843		926	
M4 Concrete	Sample 1	285	278	593	583	645	628
	Sample 2	278		576		616	
	Sample 3	271		581		623	

5. Three-Dimensional Finite Element Modeling of Tall RC Building

This study, it is aimed to examine the seismic damage performance of tall RC buildings considering the effects of granulated glass. For this purpose, a 31-story RC building is selected for 3D modeling and SAP2000 software based on the finite element method is utilized during modeling of this RC structure. Since detailed damage analysis of structures can be made with this program, the SAP2000 program is used in the study. This RC structure has a total of 4 flats on one floor. While modeling this RC structure, 6 different columns are defined to the software, and the sizes of these columns are defined as 30x50 cm, 40x75 cm, 25x40 cm, 35x60 cm, 30x40 cm, 40x40 cm, respectively. Moreover, there is a circular column in the structure and its diameter is defined as 65 cm. Then, the sizes of beams used in the three-dimensional model are defined as 25x35 cm, 30x60 cm, and 30x50 cm, respectively. The class of concrete columns and beams is defined as C25 and this value is gotten from the original structure project. In the RC structure, there is 1 shear wall and its thickness is 25 cm. Besides, the thicknesses of the floor covering are 25 cm and 20 cm for all floors. The height of each floor is 3 m and there are a total of 31 floors in the structure. In this study, the seismic behavior of the structural elements of the building is investigated and the foundation section is not modeled and fixed elements are defined on the base of the structure. Firstly, structural components are created according to the original structure project. While modeling structural components, the mass source is defined to software using dead and live loads. Furthermore, rigid diaphragms are created in the structure considering the constraint z-axis. Then, nonlinear time history analyses are performed according to the direct integration solution type. For this purpose, the Hilber-Hughes-Taylor method is taken into account in the 3D analyses and its gamma and beta value is selected as 0.5 and 0.25, respectively. 3D model of the structure is shown in Fig. 11.

6. Three-Dimensional Finite Element Analysis Results

In this study, the effects of granulated glass material, which is waste in nature, on the earthquake behavior of tall reinforced concrete buildings are discussed. After a total of 5 different concretes (pure concrete, M1, M2, M3, and M4 concretes) are prepared, the strengths of these concretes are determined. Considering these strength results, a 31-story high reinforced concrete structure is modeled as three-dimensional. The SAP2000 program-based finite-element method is used to model the building. After the structure is modeled, 5 different earthquake analyzes are performed using the 1995 Kobe earthquake. The magnitude of the 1995 Kobe earthquake is 6.9 Mw. Also, the distance of the earthquake is 0.6 km, the A_p value is 0.82g, the V_p value is 81.0 cm/s, and the T_p value is 0.9 s. Earthquake accelerations, directions, analysis type, time interval are defined to the program and earthquake analysis is started. Firstly, the modal analyzes of the structure are made and the results presented in Fig. 12 are obtained. According to Fig. 12, it is openly seen that the modal analyzes of the building are performed for 5 different concrete types. According to Fig. 12a, if pure concrete is used for the carrier elements of the structure, the natural frequency value of the structure becomes 0.285 Hz. As Fig. 12b is examined in detail, it is seen that the natural frequency value of the structure is 0.332 Hz. When this value is compared with the result obtained for the pure concrete structure, it is concluded that the M1 concrete significantly increases the natural frequency value of the structure. In Fig. 12c, the

modal behavior of the structure analyzed using M2 added concrete is presented. According to Fig. 12c, the natural frequency value acquired for the structure analyzed using M2 concrete is 0.427 Hz. As the M1 concrete with structure is compared with the M2 concrete with structure, it is understood that the M2 concrete (10% granulated glass) affects the modal behavior of the structure more. In Fig. 12d, the modal behavior of the structure analyzed with M3 concrete is presented. According to Fig. 12d, the natural frequency value gained in the structure analyzed using concrete with M3 additives is 0.591 Hz. Finally, when Fig. 12e is assessed in detail, it is seen that the natural frequency value that took place in the structure analyzed using concrete with M4 additives is 0.302 Hz.

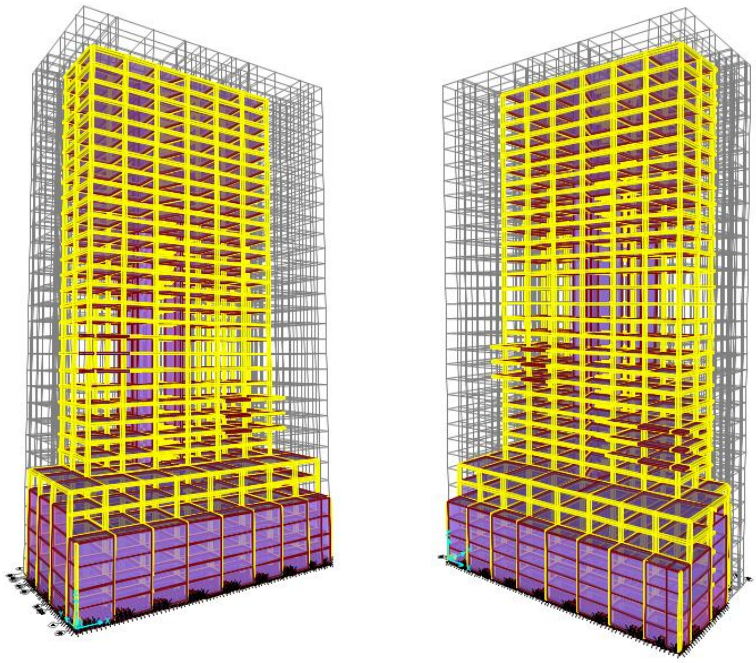

Fig. 11. Views of 3D model of the RC structure.

When the modal analysis results are compared with each other, it is openly observed that the natural frequency value that occurred in the structure analyzed with pure concrete is less than the others. This result shows that the natural period value acquired in the structure analyzed with pure concrete is higher than in the structures with granulated glass additives. Besides, the largest natural frequency value obtained for the granulated glass added structures are obtained for the structure with M3 concrete. It is clear from this result that M3 concrete has the effect of increasing the modal behavior of reinforced concrete structures more positively when compared to other additive concretes. In Fig. 13, the seismic displacement values of 5 different structures obtained as a result of seismic analyzes are presented in detail. In Fig. 13a, the earthquake analysis results of the structure analyzed with pure concrete are presented. According to Fig. 13a, it is understood that serious displacements occurred in the structure as a result of the earthquake. It is seen that the greatest horizontal displacement value in the building is 46 cm, and it is understood that this displacement took place at the top floor of the building. In Fig. 13b, the seismic analysis results acquired utilizing M1 concrete are shown. According to Fig. 13b, the largest horizontal displacements in the building occurred at the top floor of the building, and the largest horizontal displacement value gained in the building is 32 cm. Moreover, serious deformations occurred on the lower floors of the building. However, as Figs. 13a and 13b are compared with each other, it is seen that if M1 concrete is used in the building, the structure will deform less during an earthquake. This result shows that granulated glass additive affects the earthquake behavior of tall reinforced concrete buildings positively. Fig. 13c shows the seismic displacement behavior of the structure analyzed using M2 concrete. According to Fig. 13c, the largest horizontal displacement value that occurred in the building during an earthquake is 28 cm. This value took place on the top floor of the building and less seismic deformation is observed when compared to the pure concrete structure. In the structure analyzed using M3 concrete, 15 cm maximum horizontal displacement is observed and this maximum displacement occurred in the middle floors of the building (Fig. 13d). When Fig. 13e is evaluated, it is seen that the maximum horizontal displacement value obtained in the reinforced concrete building, which is analyzed considering the M4 concrete, is 38 cm. When the seismic analysis results obtained for 5 different structures are compared with each other, it is understood that the structure with the lowest displacement value is the structure using M3 concrete. In addition, the structure in which the maximum seismic deformations are obtained is the structure analyzed with pure concrete. It is clear from this result that 15% granulated glass additive affects the seismic behavior of reinforced concrete structures positively. In Figs. 14-18, the seismic M3 behavior of 5 different structures is presented. The seismic M3 values of the structure analyzed using pure concrete are shown in Fig. 14. According to Fig. 14, maximum M3 values are obtained

in the beams on the 4th floor of the building during the earthquake. The maximum M3 values occurred in the beams on the fourth floor of the building are 209 kNm, 238 kNm, and 221 kNm, respectively. In addition, serious M3 values are observed in the beams on other floors. In Fig. 15, the analysis results obtained using M1 concrete are presented. According to Fig. 15, maximum M3 values are observed in the beams on the eighth floor of the building and maximum M3 values of 182 kNm, 197 kNm, and 163 kNm are acquired in the beams on the eighth floor of the building, respectively. On the lower floors of the building, M3 values similar to the eighth floor are observed. In Fig. 16, the earthquake behavior of the structure analyzed using M2 concrete is presented. According to Fig. 16, maximum M3 values are observed in the beams on the seventeenth floor of the building. The maximum M3 values observed in the beams on the seventeenth floor of the building are 94 kNm, 83 kNm, and 75 kNm, respectively. In Fig. 17, the earthquake behavior of the structure analyzed using M3 concrete is shown in detail. According to Fig. 17, maximum M3 values are obtained in the beams on the fourteenth floor of the building and the largest M3 values that took place on the fourteenth floor of the building are 26 kNm, 32 kNm, and 42 kNm, respectively. In Fig. 18, the seismic behavior of the structure analyzed using M4 concrete is presented and the largest M3 values that occurred in the building are observed on the second floor of the building. The maximum M3 values obtained in the beams on the second floor of the building are 195 kNm, 203 kNm, and 211 kNm, respectively. Besides, serious M3 values are observed on the upper floors of the building. As the seismic analyzes of 5 different structures are evaluated, fewer M3 values are obtained in the beams of the ana-lyzed structure using M3 additive concrete compared to other structures. Besides, when 5 different structures are compared, it is understood that the M3 values in the structure using pure concrete are much higher than the other structures. In the structures analyzed with pure concrete and M4 concrete, M3 values close to each other are observed. Summary of results is shown in Table 4.

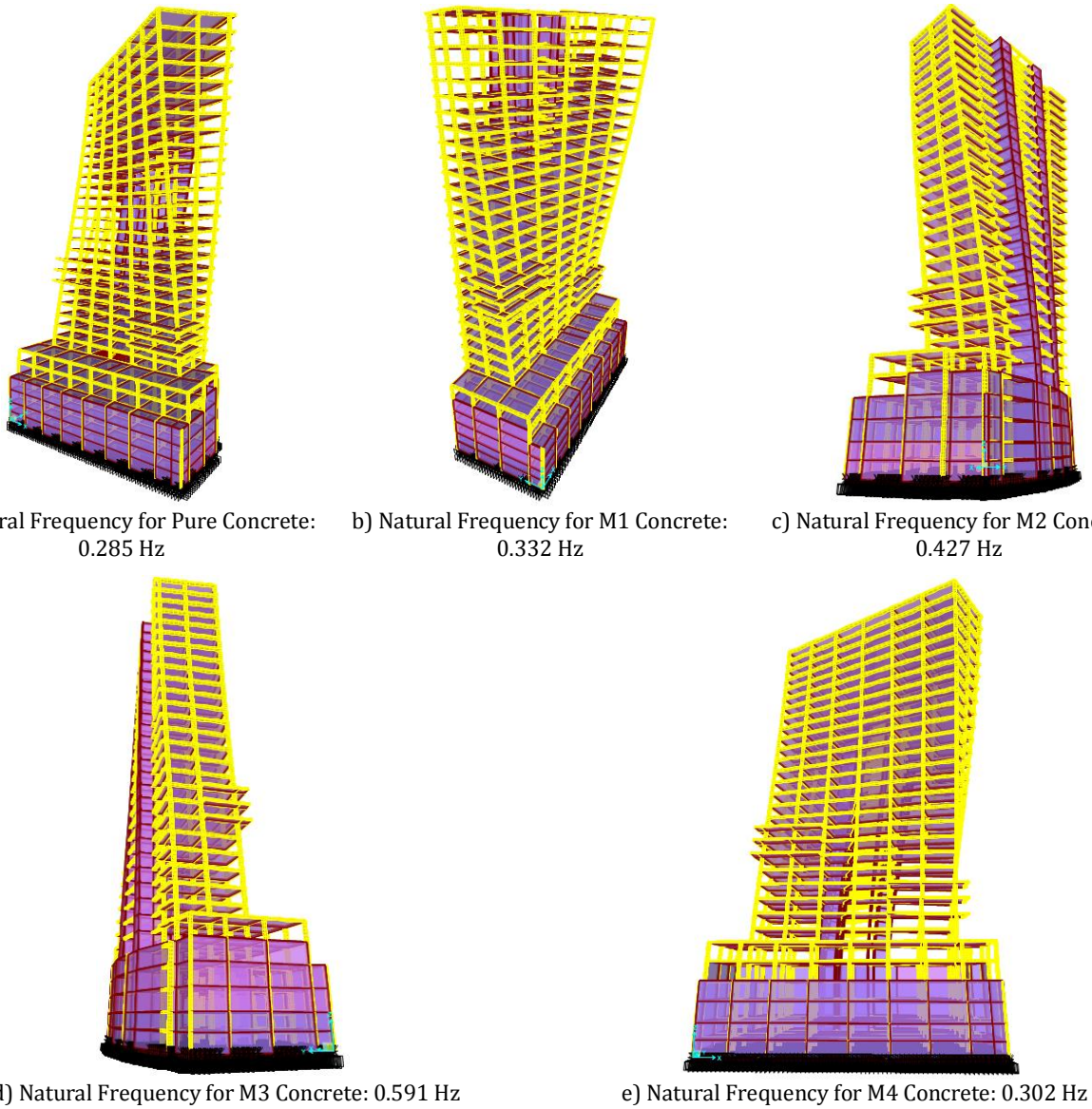

a) Natural Frequency for Pure Concrete: 0.285 Hz

b) Natural Frequency for M1 Concrete: 0.332 Hz

c) Natural Frequency for M2 Concrete: 0.427 Hz

d) Natural Frequency for M3 Concrete: 0.591 Hz

e) Natural Frequency for M4 Concrete: 0.302 Hz

Fig. 12. Modal analysis results.

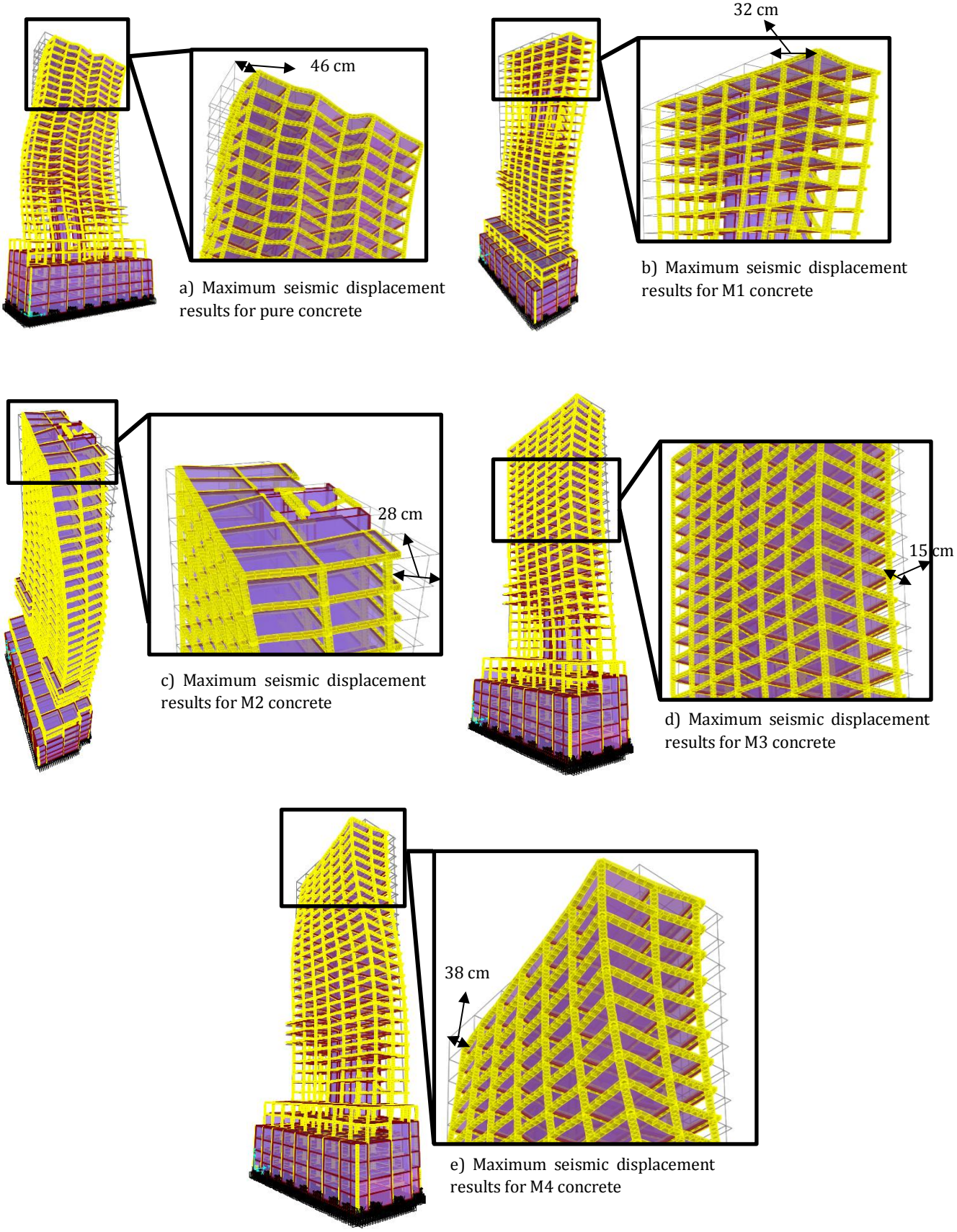

Fig. 13. Seismic displacement results for five various buildings.

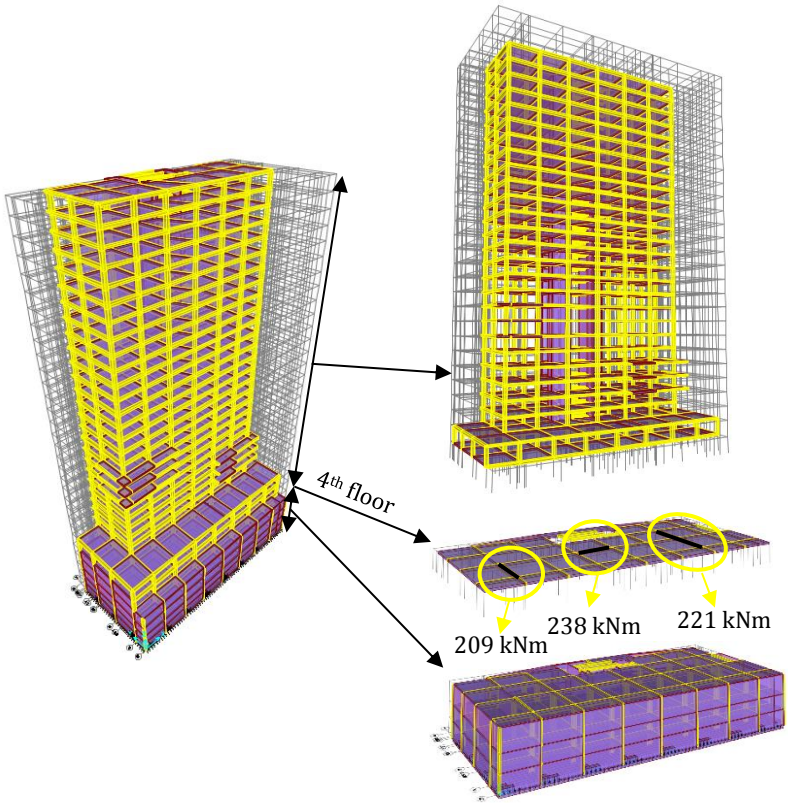

Fig. 14. Seismic principal stress results for pure concrete.

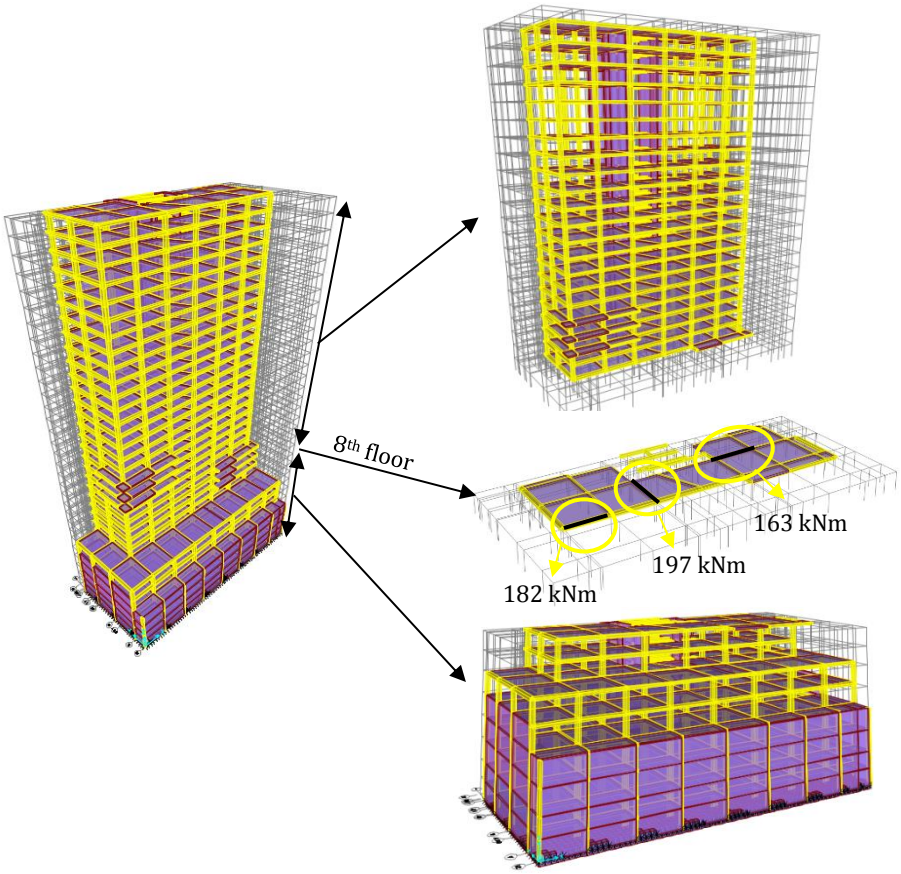

Fig. 15. Seismic principal stress results for M1 concrete.

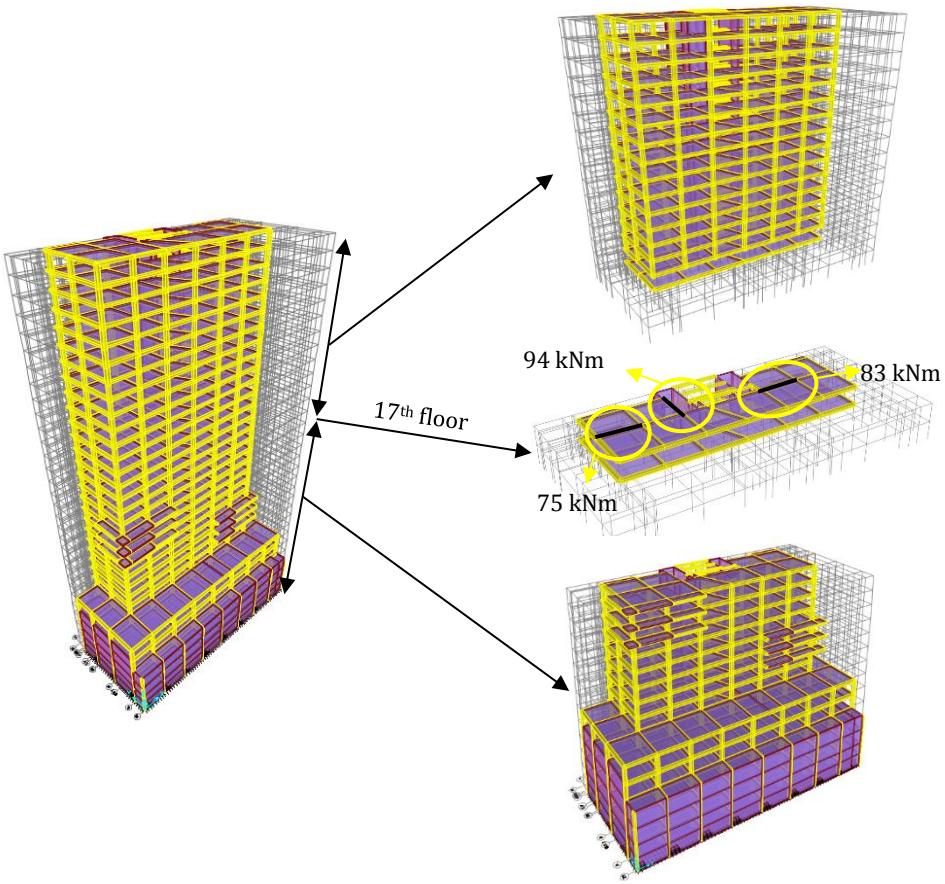

Fig. 16. Seismic principal stress results for M2 concrete.

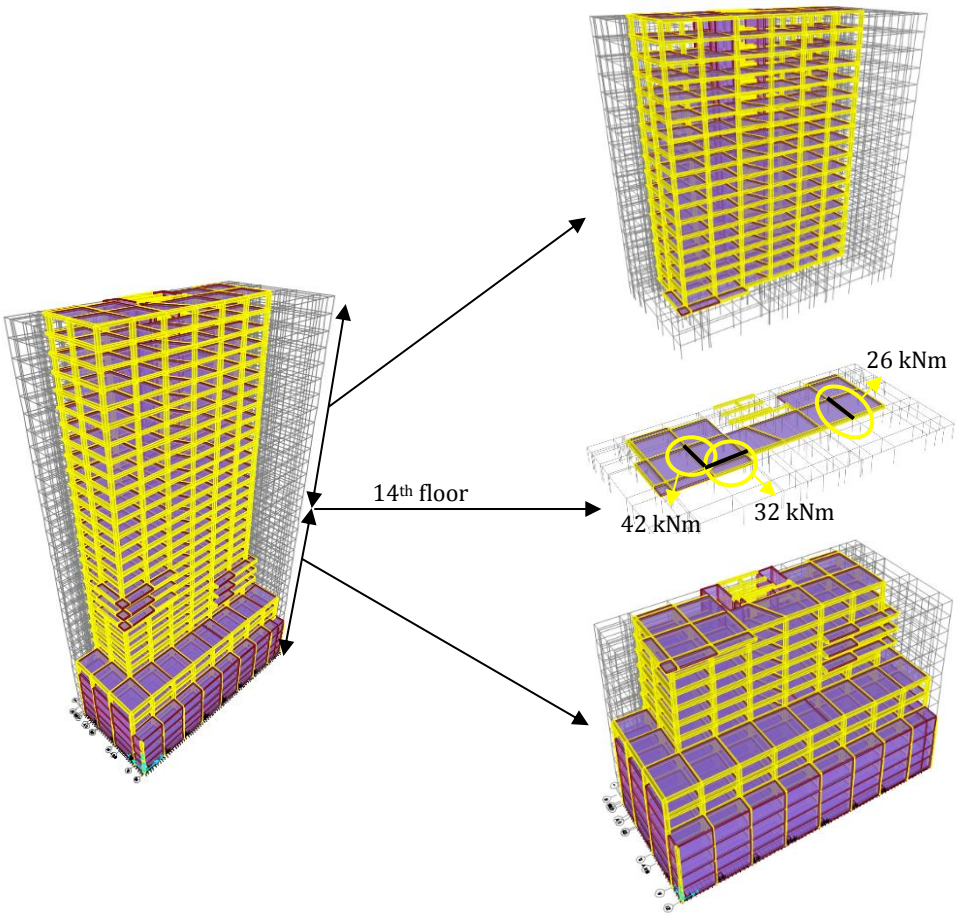

Fig. 17. Seismic principal stress results for M3 concrete.

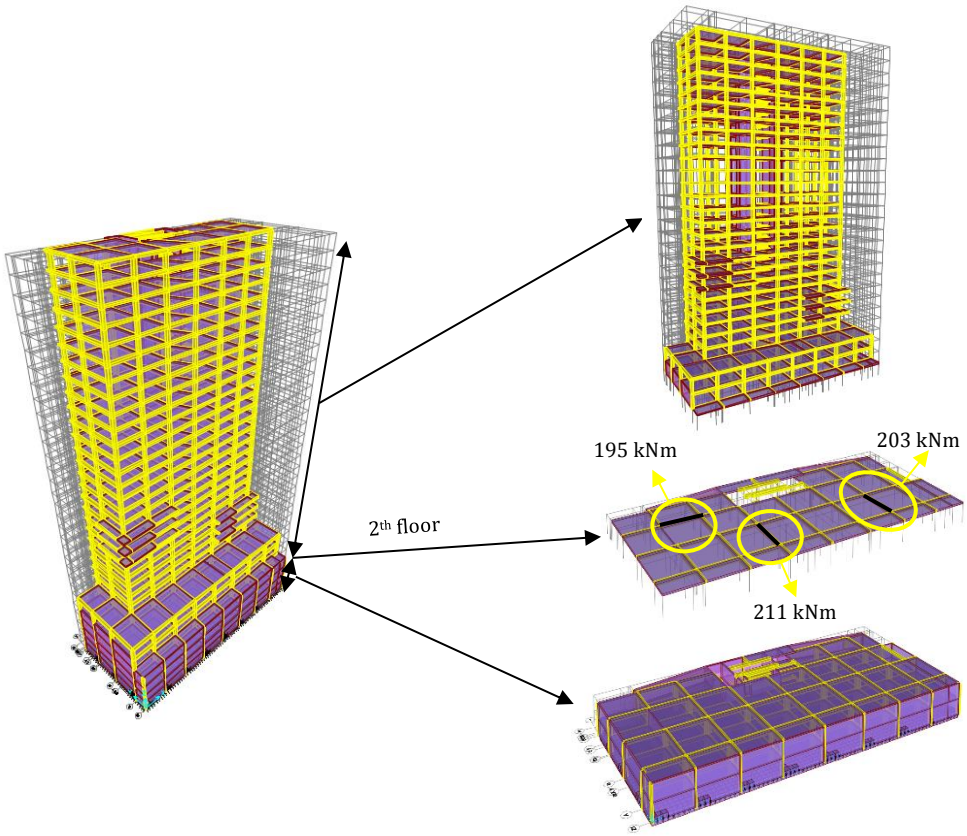

Fig. 18. Seismic principal stress results for M4 concrete.

Table 4. Summary of analysis results.

	Natural Frequency (Hz)	Max Displacement (cm)	Max Principal Stress (kNm)	Weight of Structure (t)
Pure Concrete	0.285	46	238	7267
M1 Concrete	0.332	32	197	7159
M2 Concrete	0.427	28	94	7064
M3 Concrete	0.591	15	42	6912
M4 Concrete	0.302	38	211	6833

7. Conclusions

In this study, the effects of the waste granulated glass material on the earthquake behavior of reinforced concrete structures and whether this waste material can be used in concrete materials of reinforced concrete structures are revealed. Firstly, 7-day, 14-day, and 28-day concrete samples are prepared. Pure concrete, M1 sample, M2 sample, M3 sample, and 3 cube concrete samples each from M4 samples are prepared, and these concrete samples are subjected to a compressive strength test. After the most critical granulated glass ratio is determined, a 31-story reinforced concrete structure is modeled as three-dimensional with the help of SAP2000 software. The most critical granulated glass ratio obtained is defined to the concrete material of the building. Then, the structure is subjected to earthquake analyses both as the most critical granulated glass ratio and pure concrete. 1995 Kobe earthquake is used in earthquake analyses. According to the results of the experimental and seismic analysis, the following important results are obtained.

- As a result of the experimental tests, it is seen that the granulated glass material used in concrete instead of aggregate for 15% rate increases the strength of the concrete. This result means that the granulated glass material, which is waste in nature, is recycled in the construction industry. The use of granulated glass material in reinforced concrete structures is of great importance for both our nature and our health.
- When the slump tests of pure concrete, 5%, 10%, 15%, and 20% granulated glass added to the concrete are compared with each other, it is seen that the highest amount of slump occurred as a result of the experiment is observed for 5% granulated glass added to concrete. Besides, the smallest amount of slump was obtained for 15% granulated glass added to concrete. From this result, it is understood that 15% granulated glass additive increases the consistency of pure concrete.

- In this study, it is concluded that as the waste granulated glass material is used in reinforced concrete structures, both our nature will be protected and the total weight of reinforced concrete structures will decrease. Because granulated glass material is used instead of aggregate material in concrete and aggregate material is much heavier than granulated glass material. For this reason, it has been concluded that the use of waste granulated glass material in reinforced concrete structures causes serious reductions in building weight.
- When pure concrete, 5%, 10%, 15%, and 20% granulated glass added concretes are taken into account, it is openly seen that the highest damages occurred in the tall reinforced concrete structure, which was subjected to earthquake analysis, are obtained for pure concrete. The smallest moments and displacements observed in the carrier elements of the structure are acquired for 15% granulated glass added to concrete. It is clear from this result that the use of 15% granulated glass in tall reinforced concrete structures provides positive effects in terms of earthquake resistance and earthquake damage of these structures. For this reason, in this study, it is revealed that the use of granulated glass material instead of aggregate material in reinforced concrete structures for 15% rate has positive effects on the earthquake behavior of reinforced concrete structures.

Acknowledgements

The authors would like to express thanks are to Nurettin Talha Yildiz and Uğur Konak for their helpful supports.

Funding

The authors received no financial support for the research, authorship, and/or publication of this manuscript.

Conflict of Interest

The authors declared no potential conflicts of interest with respect to the research, authorship, and/or publication of this manuscript.

References

Boukendakdji O, Kenai S, Kadri EH, Rouis F (2009). Effect of slag on the rheology of fresh self-compacted concrete. *Construction and Building Materials*, 23, 2593-2598.

Dash MK, Patro SK (2018). Effects of water cooled ferrochrome slag as fine aggregate on the properties of concrete. *Construction and Building Materials*, 177, 457-466.

El-Sayed TA (2019). Flexural behavior of RC beams containing recycled industrial wastes as steel fibers. *Construction and Building Materials*, 212, 27-38.

El-Sayed TA (2021). Performance of porous slabs using recycled ash. *Polymers*, 13, 3319.

El-Sayed TA, Shaheen YBI (2020). Flexural performance of recycled wheat straw ash-based geopolymer RC beams and containing recycled steel fiber. *Structures*, 28, 1713-1728.

El-Sayed TA, Erfan AM, El-Naby RMA (2019a). Recycled rice & wheat straw ash as cement replacement materials. *Journal of Engineering Research and Reports*, 5, 1-9.

El-Sayed TA, Erfan AM, El-Naby RMA (2019b). Flexural behavior of RC beams by using agricultural waste as a cement reinforcement materials. *Journal of Engineering Research and Reports*, 7, 1-12.

Frazão C, Díaz B, Barros J, Bogas JA, Toptan F (2019). An experimental study on the corrosion susceptibility of recycled steel fiber reinforced concrete. *Cement and Concrete Composites*, 96, 138-153.

Güneyisi E, Atewi YR, Hasan MF (2019). Fresh and rheological properties of glass fiber reinforced self-compacting concrete with nanosilica and fly ash blended. *Construction and Building Materials*, 211, 349-362.

Lynn CJ, Dhir RK, Ghataora GS, West RP (2015). Sewage sludge ash characteristics and potential for use in concrete. *Construction and Building Materials*, 98, 767-779.

Mohajerani A, Vajna J, Cheung THH, Kurmus H, Arulrajah A, Horpibulsuk S (2017). Practical recycling applications of crushed waste glass in construction materials: A review. *Construction and Building Materials*, 156, 443-467.

Nanda RP, Mohapatra AK, Behera B (2020). Influence of metakaolin and Recron 3s fiber on mechanical properties of fly ash replaced concrete. *Construction and Building Materials*, 263, 120949.

Ramdani S, Guettala A, Benmalek ML, Aguiar JB (2019). Physical and mechanical performance of concrete made with waste rubber aggregate, glass powder and silica sand powder. *Journal of Building Engineering*, 21, 302-311.

Refai AE, Abed F, Al-Rahmani A (2015). Structural performance and serviceability of concrete beams reinforced with hybrid (GFRP and steel) bars. *Construction and Building Materials*, 96, 518-529.

SAP2000. (2008). Integrated Finite Elements Analysis and Design of Structures. Computers and Structures, Inc., Berkeley, CA, USA.

Shen D, Li M, Kang J, Liu C, Li C (2021a). Experimental studies on the seismic behavior of reinforced concrete beam-column joints strengthened with basalt fiber-reinforced polymer sheets. *Construction and Building Materials*, 287, 122901.

Shen X, Chen W, Li B, Hancock CM, Xu Y (2021b). Flexural strengthening of reinforced concrete beams using fabric reinforced alkali-activated slag matrix. *Journal of Building Engineering*, 33, 101865.

Tamburini S, Natali M, Garbin E, Panizza M, Favaro M, Valluzzi MR (2017). Geopolymer matrix for fibre reinforced composites aimed at strengthening masonry structures. *Construction and Building Materials*, 141, 542-552.

Tang Z, Li W, Tam VWY, Luo Z (2020). Investigation on dynamic mechanical properties of fly ash/slag-based geopolymeric recycled aggregate concrete. *Composites Part B: Engineering*, 185, 107776.

Thorneycroft J, Orr J, Savoikar P, Ball RJ (2018). Performance of structural concrete with recycled plastic waste as a partial replacement for sand. *Construction and Building Materials*, 161, 63-69.

Uzun M, Çöğürcü MT, Keskin ÜS (2018). Effect of glass powder on concrete compressive strength. *Beykent University Journal of Science and Engineering*, 11(2), 42-51.

Wu M, Hu X, Zhang Q, Cheng W, Xue D, Zhao Y (2020). Application of bacterial spores coated by a green inorganic cementitious material for the self-healing of concrete cracks. *Cement and Concrete Composites*, 113, 103718.

Younis KH, Pilakoutas K (2013). Strength prediction model and methods for improving recycled aggregate concrete. *Construction and Building Materials*, 49, 88-701.

Xie J, Fang C, Lu Z, Li Z, Li L (2018). Effects of the addition of silica fume and rubber particles on the compressive behaviour of recycled aggregate concrete with steel fibres. *Journal of Cleaner Production*, 197, 656-667.

Zhang Q, Xiao J, Zhang P, Zhang K (2019). Mechanical behaviour of seawater sea-sand recycled coarse aggregate concrete columns under axial compressive loading. *Construction and Building Materials*, 229, 117050.